Acta Crystallographica Section D
Biological Crystallography
ISSN 1399-0047

β-Arm flexibility of HU from *Staphylococcus aureus* dictates the DNA-binding and recognition mechanism

Do-Hee Kim,[a] Hookang Im,[a] Jun-Goo Jee,[b] Sun-Bok Jang,[a] Hye-Jin Yoon,[c] Ae-Ran Kwon,[d] Sung-Min Kang[a] and Bong-Jin Lee[a]*

[a]Research Institute of Pharmaceutical Sciences, College of Pharmacy, Seoul National University, Seoul 151-742, Republic of Korea, [b]Research Institute of Pharmaceutical Sciences, College of Pharmacy, Kyungpook National University, Daegu 702-701, Republic of Korea, [c]Department of Chemistry, College of Natural Sciences, Seoul National University, Seoul 151-742, Republic of Korea, and [d]Department of Herbal Skin Care, College of Herbal Bio-Industry, Daegu Haany University, Gyeongsan 712-715, Republic of Korea

Correspondence e-mail: lbj@nmr.snu.ac.kr

Received 6 June 2014
Accepted 30 October 2014

PDB references: SHU, apo, 4qjn; DNA-bound, 4qju

HU, one of the major nucleoid-associated proteins, interacts with the minor groove of DNA in a nonspecific manner to induce DNA bending or to stabilize bent DNA. In this study, crystal structures are reported for both free HU from *Staphylococcus aureus* Mu50 (SHU) and SHU bound to 21-mer dsDNA. The structures, in combination with electrophoretic mobility shift assays (EMSAs), isothermal titration calorimetry (ITC) measurements and molecular-dynamics (MD) simulations, elucidate the overall and residue-specific changes in SHU upon recognizing and binding to DNA. Firstly, structural comparison showed the flexible nature of the β-sheets of the DNA-binding domain and that the β-arms bend inwards upon complex formation, whereas the other portions are nearly unaltered. Secondly, it was found that the disruption and formation of salt bridges accompanies DNA binding. Thirdly, residue-specific free-energy analyses using the MM-PBSA method with MD simulation data suggested that the successive basic residues in the β-arms play a central role in recognizing and binding to DNA, which was confirmed by the EMSA and ITC analyses. Moreover, residue Arg55 resides in the hinge region of the flexible β-arms, exhibiting a remarkable role in their flexible nature. Fourthly, EMSAs with various DNAs revealed that SHU prefers deformable DNA. Taken together, these data suggest residue-specific roles in local shape and base readouts, which are primarily mediated by the flexible β-arms consisting of residues 50–80.

1. Introduction

The genetic material should be folded for storage in ways that are compatible with DNA replication, chromosome segregation and gene expression. In bacteria, genomic DNA is folded into a compact structure called the 'nucleoid' (Robinow & Kellenberger, 1994; Azam *et al.*, 2000). Proteins that alter the shape of the DNA to make it more compact and that have the potential to influence transcription are termed nucleoid-associated proteins (NAPs). Several groups of NAPs have been identified in eukaryotes, archaea and bacteria. A total of 12 NAPs have been identified in Gram-negative bacteria such as *Escherichia coli* and *Salmonella enterica*; however, only six NAPs have been described in Gram-positive bacteria (Dillon & Dorman, 2010). Although several NAPs have been studied in Gram-negative bacteria such as *E. coli*, MrgA is the only functionally identified NAP among the six known NAPs (MukB, Lrp, HU, Lsr2, Hlp and MrgA) in the Gram-positive *Staphylococcus aureus*. MrgA, which is the staphylococcal Dps (DNA protection during starvation) homologue, is associated

with drastic compaction of the nucleoid under oxidative stress (Morikawa *et al.*, 2006; Dillon & Dorman, 2010).

The HU protein is the most ubiquitous and possibly the most important NAP, and determines the prokaryotic chromosome structure in both Gram-positive and Gram-negative bacteria. The members of the HU family are typically small (10 kDa), basic, heat-stable heterodimers (Gram-negative bacteria) or homodimers (Gram-positive bacteria) and function as essential proteins for bacterial nucleoids (Rouvière-Yaniv & Gros, 1975; Li *et al.*, 1999; Dame & Goosen, 2002).

HU has several DNA-related functions, such as DNA compaction, a global regulatory function of gene expression (Dame & Goosen, 2002; Sugino *et al.*, 1977) and DNA repair. HU plays dual architectural roles in relation to DNA, depending on its concentration. HU interacts with the DNA minor groove in a nonspecific manner to induce DNA bending or to stabilize bent DNA. At relatively low concentrations, individual HU dimers induce sharp DNA bends and increase its flexibility (Dame & Goosen, 2002), contributing to up to 50% of DNA compaction. At high concentrations, HU forms rigid nucleoprotein filaments (Engelhorn *et al.*, 1995). Several studies have shown that HU restrains negative supercoils in DNA. HU regulates chromosomal supercoiling by activating gyrase and by decreasing topoisomerase I activity (Drlica, 1992; Malik *et al.*, 1996).

As a global regulator, HU also influences transcription by stimulating T7 RNA polymerase (Morales *et al.*, 2002), and the transcriptional regulation of 353 genes composing 229 operons by HU has been reported (Oberto *et al.*, 2009). At the promoter, DNA supercoiling and HU promote the GalR protein to create a repression loop involved in inhibiting *gal* operon transcription (Semsey *et al.*, 2006). As an essential bacterial NAP, HU regulates the DNA-replication process and assists in the action of the DnaA protein in initiating DNA replication (Roth *et al.*, 1994; Berger *et al.*, 2010; Miller *et al.*, 2012). *E. coli* HU acts at the chromosomal replication origin (*oriC*) during replication initiation by stimulating strand opening *in vitro* (Baker & Kornberg, 1988; Skarstad *et al.*, 1990; Hwang & Kornberg, 1992), by interacting with the N-terminus of DnaA and by stabilizing the DnaA oligomer bound to *E. coli oriC* (Chodavarapu *et al.*, 2008). Several previous reports have suggested another function of HU in DNA repair. HU-deficient cells are sensitive to γ and UV damage (Boubrik & Rouviere-Yaniv, 1995; Li & Waters, 1998). HU is essential for *recA* gene-dependent DNA repair and for SOS induction pathways (Miyabe *et al.*, 2000) and can displace LexA from its binding sites on SOS-regulated operators (Preobrajenskaya *et al.*, 1994). HU preferentially binds to four-way junctions (Pontiggia *et al.*, 1993; Bonnefoy *et al.*, 1994) or to duplex DNA that contains a nick or a gap (Castaing *et al.*, 1995). HU also binds with high affinity to DNA double-strand break-repair or recombination intermediates (Kamashev & Rouviere-Yaniv, 2000). Interestingly, HU is involved in osmolarity/supercoiling responses and functions as a global regulator in the environmental programming of the cellular response during aerobic and acid stress (Oberto *et al.*, 2009). Recently, HU from *Helicobacter pylori* has been shown to act as a protector of DNA against stress damage (Wang *et al.*, 2012).

To perform these coordinated biological functions, HU should recognize and specifically bind targeted DNA. Several researchers have studied integration host factor (IHF), a homologue of HU, to elucidate its DNA-recognition mechanism. However, although IHF binds to DNA with significant sequence specificity (Engelhorn *et al.*, 1995; Ussery *et al.*, 2001), the recognition mechanism remains unclear. Serban and coworkers studied the DNA-recognition mechanism of HU from *Bacillus stearothermophilus* using Raman spectroscopy, suggesting nonspecific B-DNA minor-groove recognition (Serban *et al.*, 2003).

The mechanisms of protein–DNA interaction and recognition have been categorized as 'direct' and 'indirect' mechanisms. The mechanism commonly called 'direct readout' is based on the concept that specific recognition occurs by the formation of a series of amino acid-specific and base-specific hydrogen bonds at major grooves (Garvie & Wolberger, 2001; Viswamitra *et al.*, 1978). The term 'indirect readout' is used to describe hydrogen bonds or nonpolar interactions between proteins and DNA that require deformability of the DNA helix, such as a bend (Otwinowski *et al.*, 1988). However, these concepts do not clearly explain the mechanism of DNA recognition; thus, DNA-recognition mechanisms have recently been re-categorized as 'base' and 'shape' readouts (Rohs *et al.*, 2010). Base readout is related to base-specific or base pair-specific chemical signatures. This mechanism involves hydrogen bonds between amino acids and bases, water-mediated hydrogen bonds and hydrophobic contacts. This sequence-specific readout usually occurs on major grooves rather than on minor grooves. Shape readout is related to sequence-dependent DNA structure and deformability (Travers, 1989). Local shape readout includes local shape deviations from ideal B-DNA, such as kinks, minor-groove width and intercalation. Global shape readout involves specificity based on global DNA bending, in which the DNA backbone is in a specific conformation.

SAV1473 (molecular weight 9626 Da, 90 amino acids) is the HU protein from *S. aureus* Mu50, one of the major strains of vancomycin-resistant *S. aureus* (VRSA; Hanaki *et al.*, 1998; Howe *et al.*, 1998; Avison *et al.*, 2002). To understand the DNA-recognition mechanism of HU from *S. aureus* (SHU), the atomic structures of apo SHU and SHU–DNA must be determined. Several HU structures with and without DNA have been determined using X-ray crystallography and NMR (Tanaka *et al.*, 1984; Boelens *et al.*, 1996; Swinger *et al.*, 2003; Christodoulou *et al.*, 2003; White *et al.*, 1999), in which the proteins usually exist as dimers. Structural studies of HU proteins in the absence of DNA and the crystal structure of the HU–DNA complex showed that the structures share a common fold that consists of a large α-helical 'body' with two protruding β-ribbon 'arms'. In this study, we have determined the crystal structures of both free SHU and SHU bound to a 21 bp DNA duplex. We found structural differences between apo SHU and DNA-bound SHU and suggest that the binding

Table 1
Data-collection and refinement statistics for apo SHU and the SHU–DNA complex.

Values in parentheses are for the highest resolution shell.

Data set	Apo SHU	SHU–DNA complex
Data-collection details		
X-ray source	Beamline 26B1, SPring-8	Beamline 5C, PLS
X-ray wavelength (Å)	1.0000	0.9793
Space group	$P2_1$	$P2_12_12_1$
Unit-cell parameters (Å, °)	a = 36.63, b = 82.94, c = 60.72, β = 94.89	a = 39.47, b = 85.84, c = 92.71
Resolution range (Å)	50–2.61	50–2.16
Molecules per asymmetric unit	2 HU homodimers	1 HU homodimer, 1 DNA duplex
Observed reflections (>1σ)	65147	240585
Unique reflections	10877	17505
$\langle I/\sigma(I)\rangle$	33.7 (7.2)	69.3 (14.8)
Completeness (%)	98.8 (91.7)	99.5 (94.6)
Multiplicity†	6.0 (5.6)	13.7 (12.1)
$R_{\rm merge}$‡ (%)	8.3 (21.9)	8.8 (37.0)
Refinement statistics		
$R_{\rm work}$§ (%)	20.7	18.8
$R_{\rm free}$¶ (%)	26.3	24.9
No. of atoms		
Protein	2704	1363
DNA	—	847
Water oxygen	59	219
Average B factor (Å^2)		
Protein	41.9	29.4
DNA	—	38.6
Water oxygen	35.4	35.1
R.m.s.d.†† from ideal geometry		
Bond distances (Å)	0.009	0.007
Bond angles (°)	1.3	1.3
Ramachandran statistics, residues in (%)		
Most favoured regions	96.3	98.9
Additional allowed regions	3.4	1.1
Disallowed regions	0.3	0
MolProbity score	5.97 [99th percentile]	5.5 [98th percentile]
PDB code	4qjn	4qju

† $N_{\rm obs}/N_{\rm unique}$. ‡ $R_{\rm merge} = \sum_{hkl}\sum_i |I_i(hkl) - \langle I(hkl)\rangle|/\sum_{hkl}\sum_i I_i(hkl)$. § $R_{\rm work} = \sum_{hkl} ||F_{\rm obs}| - |F_{\rm calc}||/\sum_{hkl}|F_{\rm obs}|$ ¶ $R_{\rm free}$ was calculated identically to $R_{\rm work}$ but using 5% of the reflections that were excluded from the refinement. †† The root-mean-square deviation (r.m.s.d.) was calculated with *REFMAC*.

mode of SHU to DNA and the DNA-recognition mechanism of SHU are dictated by the flexible β-arms.

2. Materials and methods

2.1. Cloning, expression and purification of SHU

The gene encoding SHU was PCR-amplified from *S. aureus* Mu50 chromosomal DNA using the following pair of oligonucleotides: the forward primer 5′-GAATCC**CATATG**AACAAAACAGATTTAATCAATGCAG-3′ (*Nde*I site in bold) and the reverse primer 5′-CCG**CTCGAG**TTTTACAGCATCTTTTAATGCTTTACC-3′ (*Xho*I site in bold). The PCR product was digested with *Nde*I and *Xho*I and was cloned into the *Nde*I–*Xho*I-digested pET-21a (+) plasmid (Novagen Inc., Germany). The resulting construct had eight additional residues (LEHHHHHH) containing a hexahistidine tag at the C-terminus. Plasmid mutagenesis of Arg55 to Ala55, Arg58 to Ala58, Lys59 to Ala59, Arg61 to Ala61 and Pro63 to Ala63 was performed using an EZchange Site-directed Mutagenesis Kit (Enzynomics, Republic of Korea). The oligonucleotides used in the mutagenesis are listed in Supplementary Table S1[1]. The plasmid was transformed into *E. coli* BL21 (DE3) cells (Novagen, Germany). The cells were grown in Luria–Bertani medium containing 50 µg ml^{-1} ampicillin at 37°C until the OD_{600} reached 0.5–0.6, and overexpression was then induced by adding 0.5 m*M* isopropyl β-D-1-thiogalactopyranoside (IPTG). After additional incubation for 20 h at 20°C, the cells were harvested by centrifugation at 11 355*g* and frozen at −80°C. The harvested cells were resuspended in lysis buffer (20 m*M* Tris–HCl pH 7.9, 500 m*M* NaCl) and lysed by ultrasonication. The cell lysate containing SHU was centrifuged at 28 306*g* for 1 h at 4°C. The supernatant was loaded onto an open Ni^{2+}–NTA column (Qiagen, USA) and was washed with lysis buffer containing 50 m*M* imidazole. The column-bound protein was eluted using an imidazole gradient (50–500 m*M*). Finally, the buffer containing the single protein was changed to 50 m*M* Tris–HCl pH 7.5, 150 m*M* NaCl by dialysis. To perform EMSA and ITC experiments, the buffer for the wild-type (WT) SHU and the five SHU mutants was changed to 20 m*M* Tris–HCl pH 7.5, 150 m*M* NaCl. The purity of the SHU was estimated to be greater than 95% by SDS–PAGE. Because SHU has no significant absorbance at 280 nm, its concentration was determined by the Bradford assay (Hammond & Kruger, 1988), and the protein was concentrated to approximately 1 m*M* for crystallization. To conduct accurate ITC and EMSA experiments, we determined the concentration of SHU by measuring the A_{205} using the Scopes method (Scopes, 1974; Grimsley & Pace, 2004). DNA oligonucleotides, which were purified by high-pressure liquid chromatography (HPLC) or by preparative PAGE, were purchased from Bioneer (Republic of Korea) for crystallization. Single-stranded DNA (ssDNA) was solubilized in a buffer consisting of 50 m*M* Tris pH 7.5, 150 m*M* NaCl and annealed to form double-stranded DNA (dsDNA) by heating to 94°C for 5 min and then cooling to 4°C.

2.2. Crystallization

Crystals were grown by the hanging-drop vapour-diffusion method at 20°C. Briefly, 1 µl protein (1 m*M*) solution (apo) or 1 µl protein–DNA mixture (1:2 molar ratio of protein:

[1] Supporting information has been deposited in the IUCr electronic archive (Reference: MH5146).

dsDNA) was mixed with an equal volume of reservoir solution. The initial crystallization screening was performed using commercial screening kits from Hampton Research and from Emerald Bio. For apo SHU, crystals appeared in a solution consisting of 15–17.5% PEG 2000 monomethyl ether (PEG 2000 MME), 0.1 *M* Tris pH 8.5. The crystallization solution for the SHU–DNA complex was 0.4 *M* ammonium phosphate monobasic. Crystals were transferred to cryoprotectant before cooling. Cryoprotection for apo SHU was established by adding 20% glycerol to the solution and by increasing the

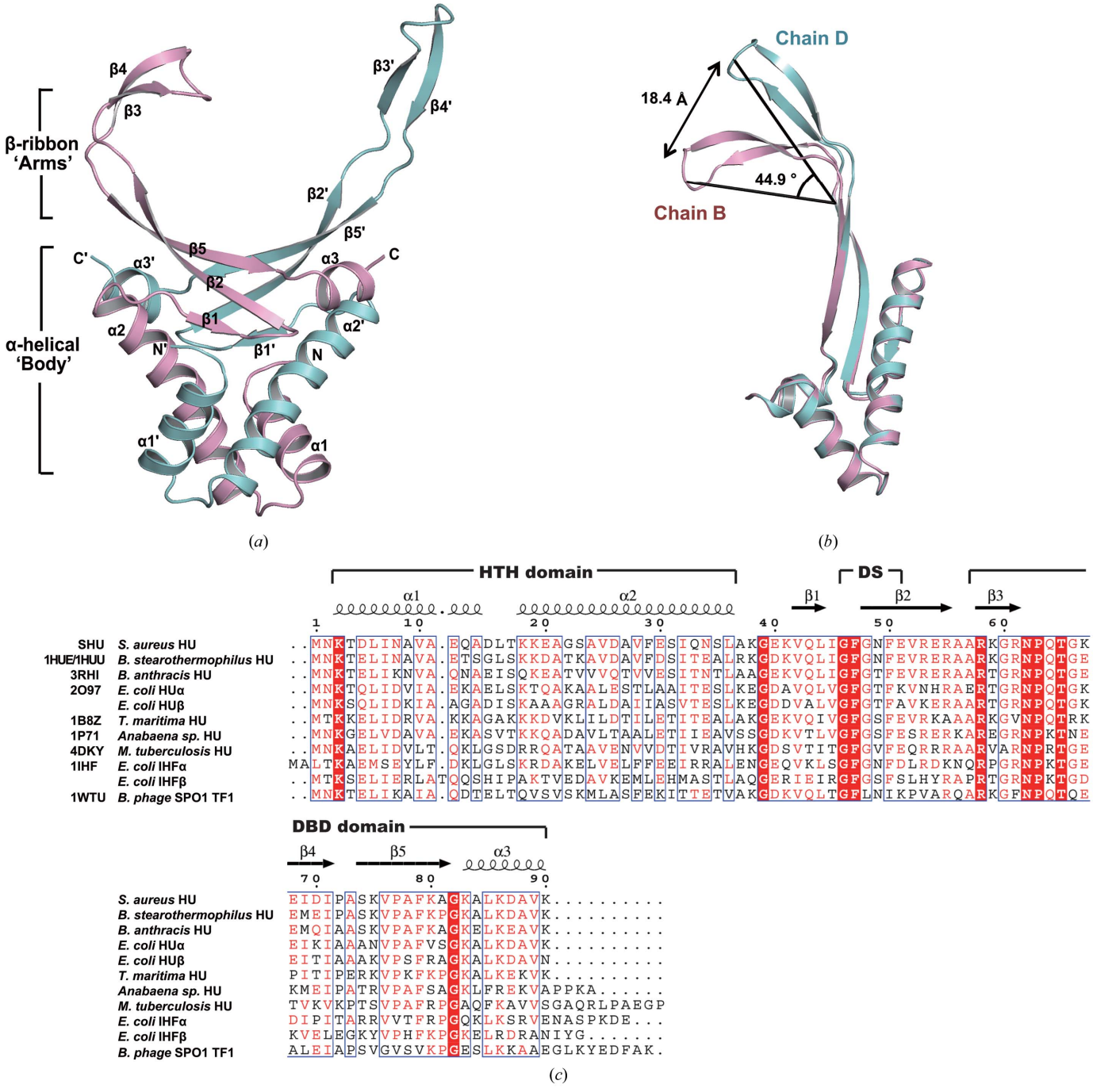

Figure 1
Structure of the apo SHU homodimer. (*a*) Ribbon diagram of the SHU homodimer. The α-helices, β-sheets and the N- and C-termini are labelled. The SHU homodimer is divided into two portions: the α-helical 'body' and the β-ribbon 'arms'. (*b*) Superimposition of chains *B* and *D* of apo SHU. The flexible β-ribbon arms deviate with a distance of 18.4 Å and with a bending angle of approximately 44.9°. The C^{α} atoms of Gln64 from each chain were used to measure the distance and bending angle, and the C^{α} atom of Arg55 from chain *D* was used as the vertex of the angle. In (*a*) and (*b*), chain *B* is shown in pink and chain *D* is shown in cyan. (*c*) Sequence alignment of SHU with homologues. Secondary-structural elements of the proteins are shown above the alignment. Highly conserved residues are highlighted in red. Alignments were generated with *ESPript* (http://espript.ibcp.fr; Gouet *et al.*, 2003).

concentration of PEG 2000 MME by 2%. Cryoprotection of the SHU–DNA crystals was achieved by adding 35% glycerol to 0.4 *M* ammonium phosphate monobasic. Crystals were flash-cooled in liquid nitrogen before data collection.

2.3. Data collection and structure determination

Data for apo SHU were collected on a Saturn A200 CCD detector system (Rigaku, Japan) at −173°C on beamline 26B1 of SPring-8, Japan. A total of 360 images were collected with 7 s exposure per frame and with an oscillation angle of 1°. The data were processed and scaled using *HKL*-2000 (Otwinowski & Minor, 1997). The space group was $P2_1$, with unit-cell parameters a = 36.63, b = 82.94, c = 60.72 Å, β = 94.9°. Data collection for the SHU–DNA complex was performed on an ADSC Quantum 315r CCD detector at −173°C on beamline 5C of Pohang Light Source, Republic of Korea. A total of 360 images were collected with 0.5 s exposure and with an oscillation angle of 1° per frame. The space group was $P2_12_12_1$, with unit-cell parameters a = 39.47, b = 85.84, c = 92.71 Å. The data-collection statistics are summarized in Table 1. To determine the structure of apo SHU, molecular replacement was performed with *PHENIX* (Adams *et al.*, 2010) using the homologous structure of the DNA-binding protein HU from *B. stearothermophilus* (PDB entry 1huu; White *et al.*, 1999) as a search model. When four molecules were assumed to be present, the Matthews coefficient was 2.30 Å^3 Da^{-1} (Matthews, 1968), with a corresponding solvent content of 46.5%. Model building was performed using *Coot* (Emsley & Cowtan, 2004), and refinement including bulk-solvent correction was performed with *REFMAC* (Murshudov *et al.*, 2011) within the *CCP*4 suite (Winn *et al.*, 2011) and with *PHENIX*. The final $R_{\rm work}$ and $R_{\rm free}$ values were 20.7 and 26.3%, respectively. The overall geometry was validated using *MolProbity* (Chen *et al.*, 2010), and 99.7% of residues were in the allowed region of the Ramachandran plot. The refinement statistics are summarized in Table 1. To determine the structure of the SHU–DNA complex, the molecular-replacement method was performed using the apo structure of SHU as a search model. After bulk-solvent correction, DNA molecules were fitted and protein and DNA molecules were refined successively using *Coot* and *PHENIX*. The model was refined further until the final $R_{\rm work}$ and $R_{\rm free}$ values reached 18.8 and 24.9%, respectively. The overall geometry was validated using *MolProbity*, and 100.0% of the residues were in the allowed region of the Ramachandran plot. The refinement statistics are summarized in Table 1. All figures were generated with *PyMOL* v.1.2r (http://www.pymol.org) and *Chimera* (Pettersen *et al.*, 2004).

2.4. Molecular-dynamics (MD) simulation

We employed the *AMBER* package (v.12) for 100 ns MD simulations (Case *et al.*, 2005). The protonation states of the protein were determined using the *PDB*2*PQR* online server (Dolinsky *et al.*, 2007). The *LEaP* program was used to set up the systems for MD simulation. Each system was solvated with TIP3P water molecules in a periodic truncated octahedral box such that its walls were at least 10 Å away from the solute. Sodium or chloride ions were added so that each system had an ionic strength of 100 m*M*. All simulations were performed with the *PMEMD* module of the *AMBER* package using the ff99SB-ILDN force field (Lindorff-Larsen *et al.*, 2010). All bonds involving H atoms were constrained by the *SHAKE* algorithm, permitting a time step of 2 fs. Nonbonded interactions were truncated at 10 Å and the particle mesh Ewald method was used to calculate long-range electrostatic interactions under periodic boundary conditions. The simulations consisted of five stages: 1000 steps of minimization, a 50 ps run for heating from 0.1 to 310 K, a 50 ps run under a constant pressure of 101.325 kPa and a temperature of 310 K, a 500 ps run for equilibration and a 105 ns run for production. Positional restraints were applied during the first three stages. Unrestrained equilibration and production runs were performed at constant temperature (300 K) using a Langevin thermostat, with a collision frequency of 2 ps^{-1}, and at constant pressure (101.325 kPa) using a Berendsen barostat, with a pressure relaxation time of 2 ps. We saved the trajectory every 10 ps for the final 100 ns of the production run for 10 000 trajectories in total. The obtained coordinates were analyzed using the *GROMACS* software suite (Van Der Spoel *et al.*, 2005). For the DNA-free and complex states, we repeated each 100 ns MD simulation three times with different random seeds for statistical analyses. We also performed MM-PBSA analyses using the *MMPBSA.py* protocol (Miller *et al.*, 2012), which is a post-processing end-state method to calculate free energy with MD trajectories of complex structures. A scheme called per-residue decomposition generated residue-specific values, where errors were calculated using the standard deviations of the free-energy values from three trajectories. Because the MM-PBSA and MM-GBSA analyses showed extremely similar patterns, we chose the values calculated by MM-PBSA for further analysis.

2.5. Isothermal titration calorimetry (ITC) measurements

ITC experiments were performed using a MicroCal 200 (GE Healthcare, Germany) at 25°C. The proteins and DNA were prepared in a buffer consisting of 20 m*M* Tris pH 7.5, 150 m*M* NaCl. An aliquot of WT SHU or SHU mutant dimers was injected into an isothermal sample chamber containing DNA oligomer solution at 150 s intervals for a total of 19 injections. Injection of SHU at the same concentration into the pH 7.5 buffer solution at 25°C was used as a blank. The MicroCal *Origin* software was used for curve fitting to calculate the binding affinity ($K_{\rm d}$), enthalpy of binding (ΔH) and entropy of binding (ΔS) and for molar ratio calculation. The raw data were fitted with one-site binding. The Gibbs free energies (ΔG) were calculated using the standard equation $\Delta G = \Delta H - T\Delta S$.

2.6. Electrophoretic mobility shift assays (EMSAs)

To distinguish the weak and strong binding of SHU to various DNAs and to elucidate the DNA binding-site size, electrophoretic mobility shift assays (EMSAs) were

conducted. dsDNA, WT SHU and the SHU mutants were prepared as described previously and the assays were performed in a binding buffer consisting of 20 m*M* Tris pH 7.5, 150 m*M* NaCl. Varying amounts of SHU protein were mixed

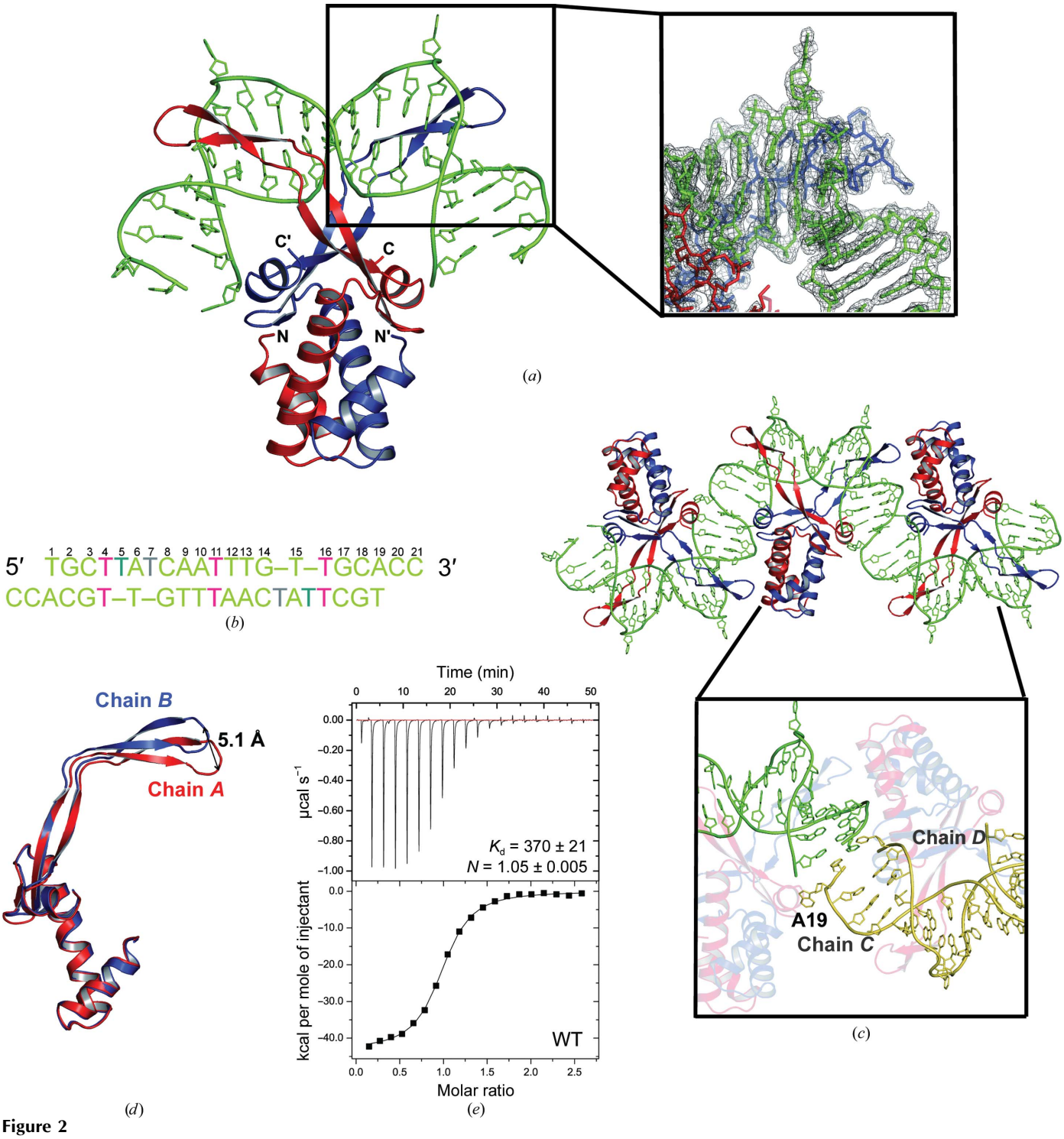

Figure 2
Structure of the SHU–DNA complex and the packing of molecules. (*a*) An SHU dimer bound to TR3 in the asymmetric unit with the $2F_o - F_c$ electron-density map contoured at a level of 1σ. (*b*) The DNA sequence of TR3 used in crystallization. The duplex of the 21-mer has mismatched and unpaired Ts. The mismatched Ts are shown in pink. Grey represents unpaired Ts that are flipped outwards and aqua represents unpaired Ts that are stacked. (*c*) Three SHU–DNA molecules arranged end-to-end form a pseudocontinuous helix in the crystal structure. An enlarged view of the stacking of DNA ends from adjacent asymmetric units is displayed in the box. DNA of a neighbouring complex is shown in yellow. Nucleotide A19 of chain *C* is flipped outwards owing to crystal-packing forces. (*d*) Superimposition of chains *A* and *B* of the SHU–DNA complex. Similar to apo SHU, the β-ribbon arms show deviations, with an r.m.s.d. of 0.54 Å and a distance of 5.1 Å at the tips (the measurement was performed as described for Fig. 1*b*). In all panels, chain *A* of the complex is in red, chain *B* is in blue and TR3 is in green. (*e*) ITC analysis of SHU–TR3 binding. The observed *n* value of 1.05 reflects that one dsDNA binds one SHU dimer.

with DNA to give a final volume of 6 µl and incubated for 20 min at 4°C. The total binding solutions were loaded onto 0.8% agarose gels in 0.5× TBE (45 m*M* Tris-borate, 1 m*M* EDTA) buffer or onto 7%(*w*/*v*) nondenaturing polyacrylamide gels in 1× TBE for electrophoresis, and the results were visualized using a Gel Doc (Bio-Rad).

2.7. DNA angle calculation

Bend angles and dihedral angles were determined by slight modification of a previously described method (Swinger *et al.*, 2003). DNA was roughly divided into three straight helices with two bending sites, and three lines representing three helices were denoted as lines *a*, *b* and *c*. Lines *a*, *b* and *c* contained the T1:T4, A9:T13 and T16:C18 base pairs from chain *C*, respectively. Three best-fit lines, the linear helical axes defined by equivalent C1′ and RN9/YN1 atom pairs, were calculated using the *w3DNA* web server (Zheng *et al.*, 2009). Bend angles 1 and 2 were calculated between lines *a* and *b* and between lines *b* and *c*, respectively, using the formula below. The overall bend angle was determined using lines *a* and *b* and was not a simple sum of angles 1 and 2 because the DNA was not positioned in a co-plane. The dihedral angle was calculated using the formula below with the results from the cross-product between lines *a* and *b* and lines *c* and *b*. The angles of *Anabaena* HU (AHU) were calculated using the same methods as for SHU; however, line *c* contains the T16:A19 base pairs.

$$\alpha = \cos^{-1}[(\mathbf{l1} \cdot \mathbf{l2})/(|\mathbf{l1}||\mathbf{l2}|)]. \quad (1)$$

3. Results

3.1. Overall structures of apo SHU and the SHU–DNA complex

The asymmetric unit contains four HU polypeptide chains arranged as two dimers: chains *A* and *C* and chains *B* and *D*. The physiologically relevant SHU dimer is identified in the structure in Fig. 1(*a*). The topology of the HU monomer is represented in Fig. 1(*c*) and includes three α-helices and five β-sheets arranged in the order α1–α2–β1–β2–β3–β4–β5–α3 in the secondary structure. Each monomer of the HU molecule is divided into three portions (Christodoulou *et al.*, 2003; Christodoulou & Vorgias, 2002): the helix–turn–helix (HTH) domain, the dimerization signal (DS) and the DNA-binding domain (DBD) (Fig. 1*c*). The SHU homodimer forms a V-like body that is divided largely into two parts: an α-helical body and two protruding β-ribbon arms (the dimerization interface of apo SHU is described in the Supporting Information). The sequence of the β-ribbon arm is highly conserved, including the consensus RNP motif at the tip of the DNA-binding arms (residues 61–63; Grove & Lim, 2001), and is enriched in basic amino acids. The monomers are not identical (asymmetric), even though HU is a homodimer. Chains *A* and *B* and chains *C* and *D* showed similar positioning of the β-arms, which are bent by approximately 44.9°. Although the α-helical body superposed well, each monomer of the SHU structure had a different magnitude of β-ribbon arm bending, with a root-mean-square deviation (r.m.s.d.) value of 0.25 Å for 68 C^{α} positions, as shown in Fig. 1(*b*) and Supplementary Table S2. Chains *B* and *D* were used as the representative dimer structure for analyzing apo SHU.

Previous studies revealed that HU, which binds particularly tightly to structurally distorted DNA such as nicks or four-way junctions, performs an architectural role by binding to various target DNAs (Pontiggia *et al.*, 1993; Bonnefoy *et al.*, 1994; Castaing *et al.*, 1995). To understand how HU works in DNA binding and recognition and the role of its flexible β-arms, we co-crystallized SHU with dsDNA. We attempted to grow crystals with several types of DNA; however, we only obtained crystals with TR3 dsDNA, which was used in the AHU–DNA study (Swinger *et al.*, 2003). TR3 is a pseudo-self-complementary duplex with sequence TGCTTATCAATTTGTTG-CACC (Fig. 2*b*). The sequence features three T:T mismatches and four unpaired Ts, without which crystallization was unfavourable. In the SHU–DNA structure, the asymmetric unit contains one protein dimer and one dsDNA (Fig. 2*a*). Overall, the β-arms of the HU homodimer form a saddle-like surface; dsDNA penetrates through this surface and the β-arms clamp dsDNA along the minor groove. The structure of the SHU–DNA complex also exhibits asymmetry, although the protein and DNA duplex are homodimers. Part of the crystal packing with three asymmetric units of the molecules is shown in Fig. 2(*c*) and the dsDNA from the adjacent asymmetric units forms a pseudocontinuous helix. Superimposition of each monomer demonstrates the difference in each structure (a distance of 5.1 Å at the tips), as shown in Fig. 2(*d*). Compared with the apo SHU structure, the basal secondary structure is maintained, and the partially disordered β-arms are stabilized by crystal contacts with the DNA. However, a conformational change occurs in the DNA-embracing β-strands, which fold upon DNA binding. The detailed DNA interactions are described below.

3.1.1. Structural comparison of apo SHU with other homologues. The SHU molecule structure shares an overall unique fold with previously reported HU homologue structures. Closely related structures are those from *B. anthracis* (PDB entry 3rhi; Center for Structural Genomics of Infectious Diseases, unpublished work), *E. coli* (PDB entry 2o97; Guo & Adhya, 2007), *Thermotoga maritima* (PDB entry 1b8z; Christodoulou & Vorgias, 1998), *B. subtilis* phage SPO1 (PDB entry 1wtu; Jia *et al.*, 1996), *B. stearothermophilus* (PDB entries 1hue and 1huu; Vis *et al.*, 1995; White *et al.*, 1989) and *Mycobacterium tuberculosis* (PDB entry 4dky; Bhowmick *et al.*, 2014). A comparison of the structures of several HU homologues is presented in Supplementary Table S2. Overall, SHU shows moderate to high sequence identity to the other homologues. Interestingly, when the overall structures of whole HUs are compared the α-helical body seems to superpose well; however, the β-arms do not conform to each other, presumably owing to their flexibility, with the exception of transcription factor 1 from *B. subtilis* phage SPO1 (Supplementary Fig. S2*a*). The flexibility of HU β-arms is represented

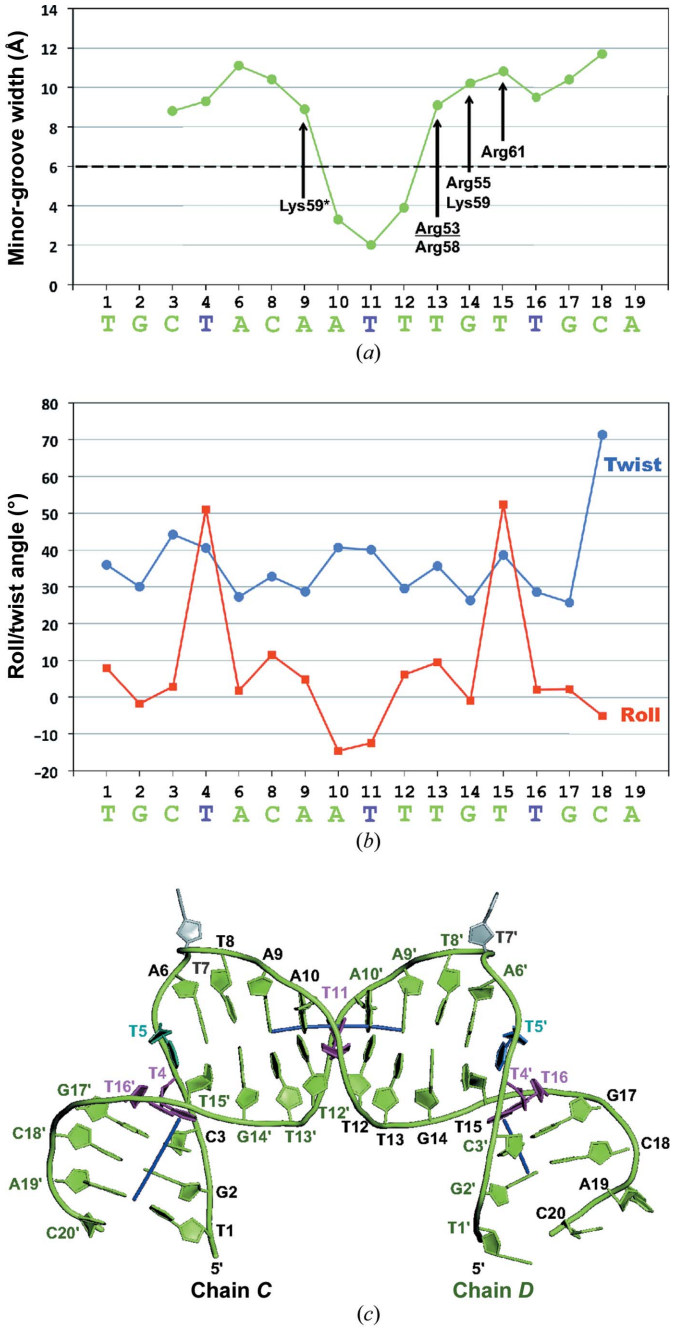

Figure 3
The structural distortions in the SHU-bound DNA. (*a*) Minor-groove width calculated using the *Curves*+ algorithm. The dashed line denotes canonical minor-groove widths from B-form DNA. The basic residues that interact with the base are indicated by arrows. Lys59, which is involved in water-mediated hydrogen bonding, is marked with a star. Arg53, which forms a nonbonded contact to a phosphate group, is underlined. Arg61, which forms a hydrogen bond to T5, is not represented. (*b*) Roll and twist angles at the base-pair steps calculated using the *w3DNA* web server (the unpaired T5 and T7 were excluded from the calculations). (*c*) DNA in the SHU–DNA complex. The nucleotides of chains *C* and *D* are shown in black and green, respectively. The axes are represented as blue lines and mismatched or unpaired nucleotides are coloured as in Fig. 2(*b*). The central segment A10-T11-T12 of DNA exhibits a narrow minor groove, a negative roll angle and an overtwisted angle. The large roll-angle deviation and overtwisted angle at T4–C8, T14 and G16 correspond to the DNA kink. Arg61 plays a crucial role in stabilizing and recognizing DNA at the kink as well as a role in DNA binding.

Table 2
Bending angles at each kink, overall bend angles and dihedral angles for SHU-bound and AHU-bound DNA.

The angles were calculated according to the method described in §2.

	Angle 1 (°)	Angle 2 (°)	Overall bend (°)	Dihedral (°)
SHU-bound DNA	62	63	124	8
AHU-bound DNA†	52 (74)‡	75 (84)	120 (106)	30 (72)

† DNA from PDB entry 1p71. ‡ An angle that was determined in a previous report (Swinger *et al.*, 2003).

by the observation that these structures are frequently disordered in previously characterized apo structures. The structures from *B. stearothermophilus* and *B. subtilis* phage SPO1 also exhibited flexible β-arms. The other structures possessed unstructured β-arms that were not detected, except for in the HUs from *M. tuberculosis* and *S. aureus*.

3.1.2. DNA conformation. Both the global and the local shape of DNA contribute to protein–DNA binding specificity, cooperativity and affinity (Rohs *et al.*, 2009, 2010). To analyze the topology of SHU-bound TR3, we used the *w3DNA* web server (Zheng *et al.*, 2009) and the *Curves*+ algorithm (Lavery *et al.*, 2009). At the DNA site where the β-strands of SHU are bound, DNA bending is maximal, yielding an overall curvature of ∼119°. The bending angles and overall bending angles are listed in Table 2. The local base-pair steps at T4:A6 and T15:T16 exhibit large positive roll angles (49.7 and 50.8°, respectively) and are overtwisted, with two kinks in the region that divides TR3 into three roughly linear B-form helices (Figs. 3*b* and 3*c*). This bendability of DNA with suitable spacing is a crucial component of protein recognition. The large roll angle of DNA in the minor groove could be explained by the finding that the pyrimidine/purine steps tend to cause positive roll bending (Dickerson, 1998). The Pro63 ring and the guanidinium side chain and amide backbone N atom of Arg61 affect the local helical structure, which is represented by large roll angles.

Interestingly, the bending and dihedral angles are slightly different from those in the AHU–TR3 complex, although these angles possess identical DNA sequences. The differences between SHU and AHU may originate from their local molecular environments during crystal stacking (a detailed explanation is discussed in the Supporting Information) and the binding properties of HUs may originate from the local sequence difference in the β-arm region. In AHU, Lys56 and Glu59 replace the conserved Ala56 and Lys59 of SHU, respectively. Lys56 of AHU in the flexible hinge region may hinder β-arm bending when compared with Ala56 in SHU, reducing DNA distortion. Lys59 in SHU, which corresponds to Glu59 in AHU, could contact the DNA, possibly accelerating the conformational change in both the β-arms and the DNA in SHU.

Rhos and coworkers suggested that the shape of the minor groove, which has a narrow width and a negative electrostatic potential, is readily recognized by a complementary set of basic side chains, typically Arg (Rohs *et al.*, 2009). To determine the relationship between the minor groove and basic residues, the minor-groove width was calculated using the

Curves+ algorithm (Lavery *et al.*, 2009). In our structure, a distinctive feature of the DNA conformation is the compressed minor groove in the centre of TR3, which is compensated by the wide minor-groove width at the binding site near the kinks where the interactions with the arginine residues are primarily observed (Fig. 3*a*). This wide minor-groove width is a critical property of SHU, which provides a favourable condition for the β-strand arms of the SHU dimer to be inserted into the adjacent minor groove with presumably higher binding affinity for TR3.

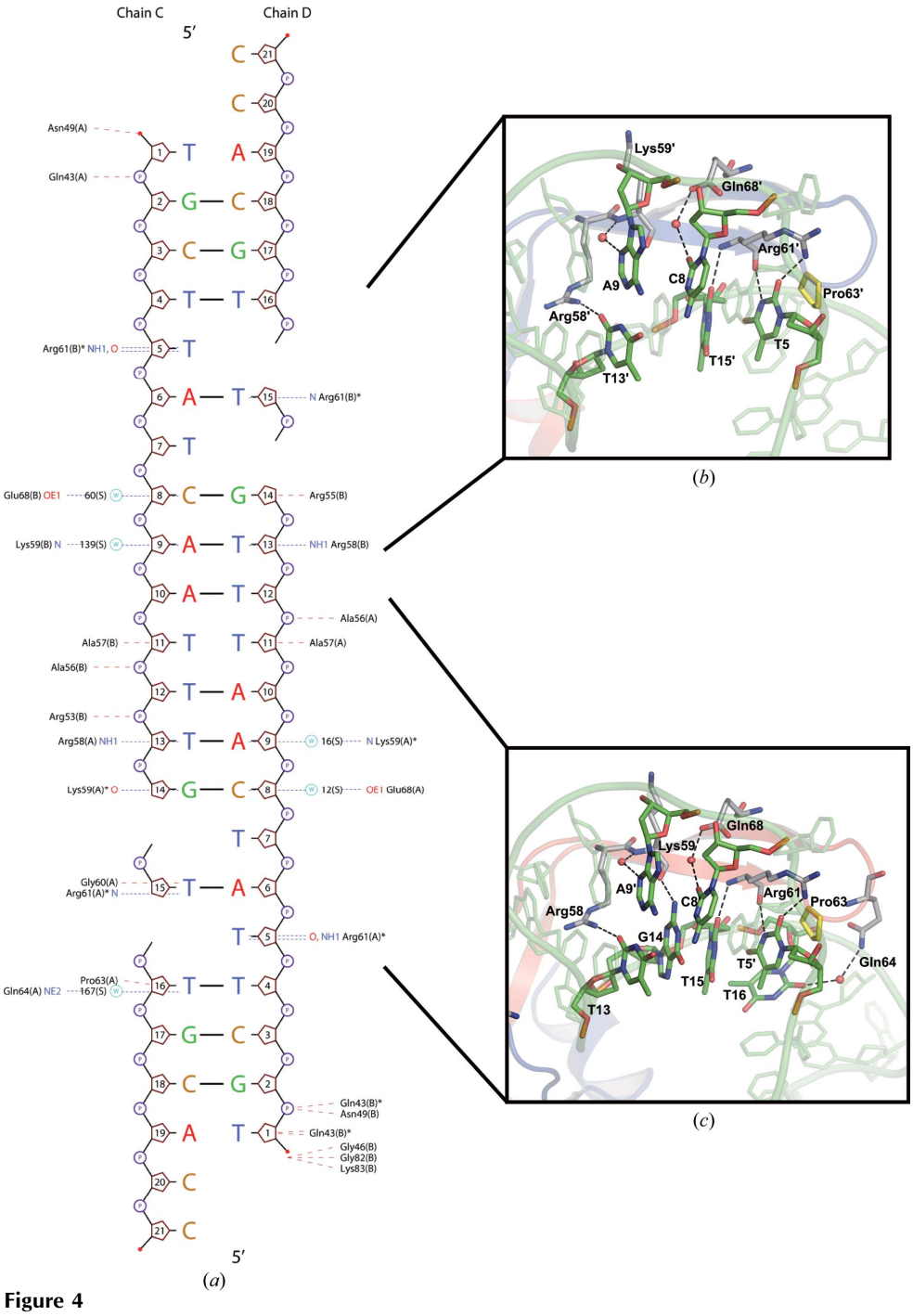

Figure 4
The contacts between the SHU protein and TR3 DNA. (*a*) Schematic diagram of the SHU–DNA contacts. The deoxyribose of each nucleotide is numbered, labelled and shown as a pentagon. Hydrogen bonds to the bases and phosphate backbone are shown as blue dashes and hydrophobic contacts (<3.35 Å) are shown as red dashes. Residues and atoms involved in interactions are labelled. (*b*) Detailed view of the SHU–DNA contacts. The residues and DNA involved in hydrogen bonds are shown in stick representation. The backbone C atoms of the protein are shown in grey and the backbone C atoms of DNA are shown in green. Other atoms are coloured as follows: red, oxygen; blue, nitrogen; yellow, sulfur. The basic residues Arg and Lys directly contact the DNA base. Arg61, in concert with Pro63, plays a crucial role in recognizing and stabilizing DNA.

3.1.3. Protein–DNA interface in the SHU–DNA complex. Some architectural proteins are known to only contact the minor groove of DNA. This interaction occurs with extensive hydrophobic contacts and a dramatic widening of the minor groove (Bewley *et al.*, 1998). This base readout is also observed in the SHU–DNA complex structure. SHU–dsDNA interactions, which include hydrogen-bonding and hydrophobic interactions between the protein and the DNA, were analyzed using the *NUCPLOT* program (Luscombe *et al.*, 1997) and are shown in Fig. 4(*a*). Among the 42 bound nucleotides, only 21 nucleotides make 31 contacts with 16 residues, mainly on the β-arm region of SHU. The majority of the interactions between SHU and DNA involve amino acids in the β-arm region, *i.e.* Arg53, Ala56, Ala57, Arg58 and Arg61, which are conserved in SHU homologues (Fig. 1*c*). The middle narrow minor-groove region forms hydrophobic contacts with Arg53, Ala56 and Ala57. The water molecules that displace the amino acids in the narrow minor-groove region provide the thermodynamic driving force for DNA binding to Lys59 and Glu68. Direct contacts with DNA bases in the minor groove are formed by Arg58, Lys59 and Arg61. The O atom of Lys59 in chain *A* accepts a hydrogen bond from the N2 atom of G14. Arg58 and Arg61 are highly conserved and play crucial roles in DNA recognition and binding. The flexibility of the β-ribbon arms allows the guanidinium side chain of Arg to realign and form suitable contacts with DNA. The side chain (NH1)

of Arg58, which is conserved in all SHU homologues, is inserted into the minor groove and is involved in a hydrogen bond to the O2 atom of T13. Additionally, the DNA kink regions at the unpaired 5T of each complementary strand are 9 bp apart (Figs. 4*b* and 4*c*) and come into contact with the highly conserved RNP motif (residues 61–63). Arg61 of the RNP motif is crucial for DNA recognition. The guanidinium side chain of Arg61 penetrates deeply into the DNA minor groove, forming several interactions. The NH1 and O atoms of the Arg61 side chain from each SHU subunit form hydrogen bonds to the O2 and N3 atoms of 15T, respectively. The amide N atom of Arg61 makes contacts with the O2 atom of T5′ of the complementary strand. Pro63 makes nonbonded contacts with the sugar groups and rings of the adjacent T16, intercalating in the minor groove. These interactions stabilize kinked DNA, causing deformation of the DNA helix such as DNA bending. Previous IHF–DNA and AHU–DNA complex structures have demonstrated such interactions (Rice *et al.*, 1996; Swinger *et al.*, 2003), supporting the notion that DNA–RNP motif binding contributes to the stabilization of DNA bending.

Table 3
Thermodynamic parameters for SHU–TR3 binding (298 K, 20 m*M* Tris pH 7.5, 150 m*M* NaCl).

ND, not determined.

SHU (SHU:TR3)	*n*	K_d (n*M*)	ΔH (kcal mol^{-1})	$T\Delta S$ (kcal mol^{-1})	ΔG (kcal mol^{-1})
Wild type (150:12 μ*M*)	1.05 ± 0.005	370 ± 21	−41.1 ± 0.2	−2.7	−38.4
Arg55Ala (125:10 μ*M*)	1.21 ± 0.063	6725 ± 991	−83.2 ± 2.1	−6.4	−76.8
Arg58Ala (150:12 μ*M*)	0.900 ± 0.021	421 ± 105	−65.2 ± 1.8	−4.8	−60.4
Lys59Ala (150:10 μ*M*)	0.575 ± 0.013	1616 ± 300	−99.3 ± 3.1	−7.7	−91.6
Arg61Ala (150:10 μ*M*)	ND	ND	ND	ND	ND
Pro63Ala (150:10 μ*M*)	ND	ND	ND	ND	ND

To evaluate the protein–DNA interactions at the β-arms, we produced five SHU mutants (R55A, R58A, K59A, R61A and P63A) and analyzed their binding abilities using ITC and EMSAs. The R61A and P63A mutants showed moderately reduced affinities for oligomer No. 2 compared with other mutants in EMSA experiments (Supplementary Fig. S4*a*). However, affinity measurements using ITC were impossible owing to the very weak affinities (Supplementary Fig. S4*c*). Additionally, the R55A and K59A mutants also showed reduced affinity in EMSA and ITC experiments (Table 3, Supplementary Fig. S4*c*). The R58A mutant also showed a relatively high K_d value compared with that of WT SHU, representing a reduced binding affinity. These results suggest that these five residues are crucial for protein–DNA interactions, especially Arg61 and Pro63. The detailed results are discussed in §3.3.3.

Additionally, the Gln43 side chain from strand β1 forms a nonbonded contact with the adjacent O2P atom of G2, and Asn49 from strand β2 of monomer *A* forms nonbonded contact with T1 of DNA duplex chain *C*. Interestingly, A19 of chain *C* is flipped outwards, in contrast to A19 of chain *D* (Fig. 2*c*). Consequently, T1 of chain *D*, which is the pairing partner of A19 of chain *C*, interacts with the amide N atom of Gly46 and Lys83 of chain *B* by nonbonded contacts.

3.2. Dynamic protein properties upon DNA binding

3.2.1. Disruption and formation of salt bridges coupled with DNA binding. SHU has 31% charged residues, including His, Arg, Lys, Asp and Glu, which is similar to the charged-residue content of mesophilic homologues (Christodoulou *et al.*, 2003). The charged residues are exposed on the surface. Multiple salt bridges are observed in the apo SHU and SHU–DNA complex structures (Supplementary Fig. S6). Usually, DNA binding is coupled with the disruption of salt bridges in proteins because the DNA-binding interfaces of proteins are affected by the negative charge of the DNA phosphate backbone. The positively charged residues on the surface are complementary to the DNA surface. In SHU, both the disruption and the formation of salt bridges accompany DNA binding (Supplementary Fig. S6). All of the Lys–Glu salt bridges are broken upon DNA binding. The salt bridge between Lys3 and Asp26, which clamps helix 1 and helix 2, and the salt bridges between Lys83 and Asp87 and between Lys90 and Asp87, positioned at helix 3 near the end of dsDNA, are maintained. In both β-ribbon arms the salt bridges between Lys59 and Asp70 are also maintained upon DNA binding, in spite of the change in distance. The salt bridge between Lys75 and Glu54 is broken upon DNA binding, and a salt bridge is formed between Lys80 and Glu51. The salt bridges that connect β1 and β2 are broken upon DNA binding.

3.2.2. MD simulations and dynamic protein properties. To study the structural dynamics of the protein–DNA complex, the apo SHU and SHU–DNA complex structures were used in a molecular-dynamics simulation for 100 ns. The MD analyses of apo SHU and the SHU–DNA complex were repeated three times each. Supplementary Fig. S8(*a*) shows the r.m.s.d. variation in the two structures for 100 ns. For apo SHU, the C^α r.m.s.d. fluctuated in the range 4 ± 2 Å. For the SHU–DNA complex, the C^α r.m.s.d. was 1.5 ± 0.5 Å, which indicates that the SHU in the SHU–DNA complex is more dynamically stable than apo SHU. This result is complemented by the radius of gyration (R_g), which indicates the structural compactness over the trajectory and is calculated in Supplementary Fig. S8(*b*). The overall R_g value is similar between the apo and DNA-bound SHU structures, implying a similar compactness. However, the R_g of the SHU–DNA complex exhibits a more stable value (1.95 nm) than that of apo SHU, as shown in the r.m.s.d. plot. Furthermore, we determined the structural stability of the residues that primarily contribute to the binding by calculating the root-mean-square fluctuation (r.m.s.f.; Supplementary Fig. S8*c*). The residues showing large deviation values coincide with the residues in the bending region of SHU, *i.e.* residues 50–80. In particular, the residues of apo SHU with large values indicate that apo SHU is more dynamic than the SHU molecules of the SHU–DNA complex.

The flexible β-ribbon arms of SHU most likely become more stable and compact on binding to DNA. To further investigate the detailed SHU–DNA interaction, the binding free energies in the SHU–DNA complex were decomposed on a per-residue basis using the MM-PBSA approach (Fig. 5*a*). Large values of ΔG are found in the regions around the β-arm. Specifically, large changes were found for the residues Arg53, Arg55, Arg58, Lys59 and Arg61. The basic residues are aligned on a single face contacting DNA, and Arg55 is positioned in the hinge region of the β-arm. Among these basic residues, Arg61 shows the largest change, suggesting that Arg61 is essential for DNA binding and recognition.

3.2.3. Domain motion involved in DNA binding. The DNA-embracing β-arms of SHU are folded upon binding to DNA. The overlaid structures of apo SHU and the SHU–DNA complex are shown in Figs. 5(*c*) and 5(*d*). Structural comparison between apo SHU and DNA-bound SHU showed that the α-helical body remained essentially identical, with an

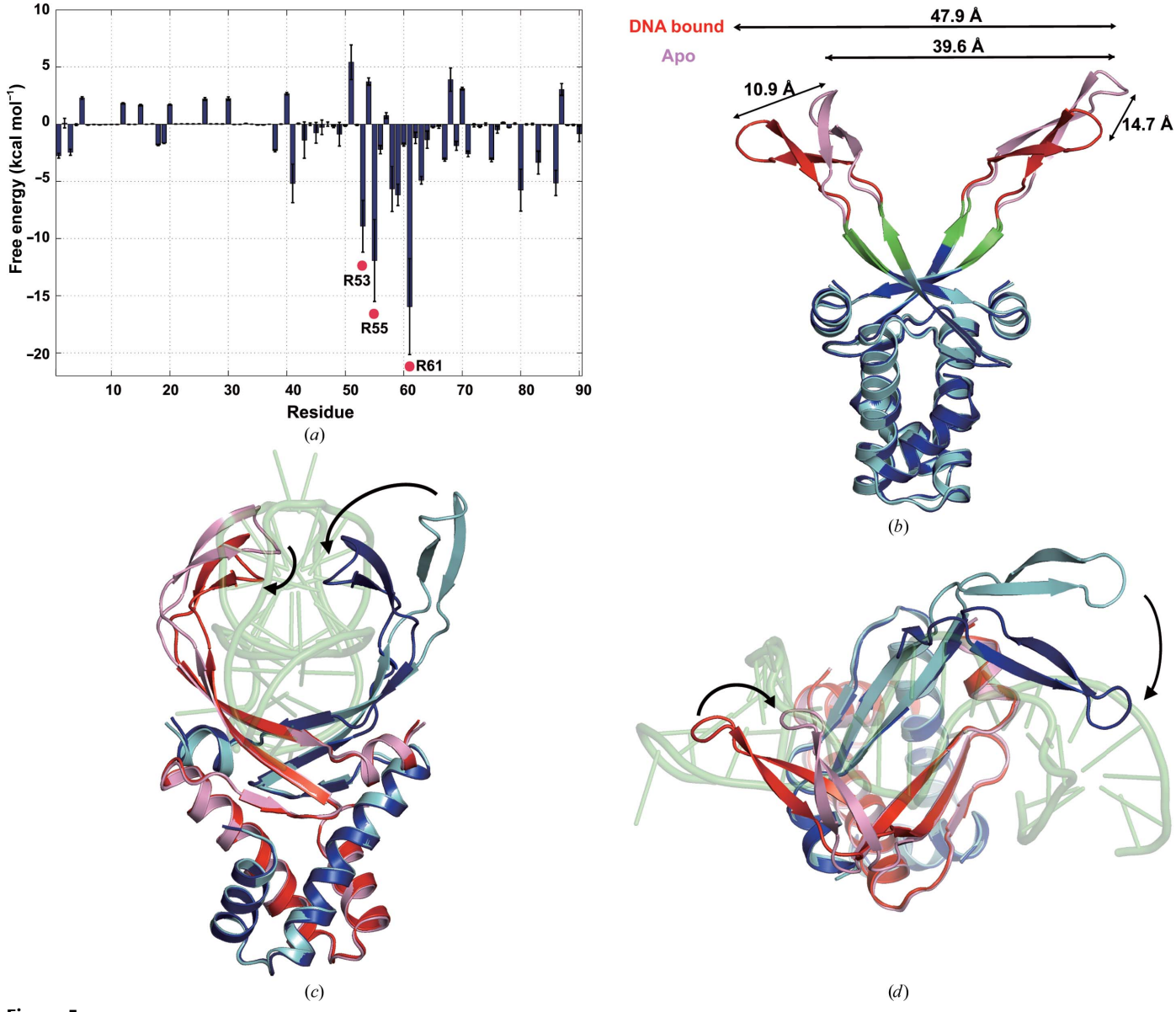

Figure 5
The structural dynamics and conformational changes of SHU upon DNA binding. (*a*) The binding free energies in the SHU–DNA complex, as determined by MD simulation. The three Arg residues (Arg53, Arg55 and Arg 61) that show low free energies are marked with red circles. Arg61 shows the lowest free energy, which suggests an essential role of this residue in recognizing and binding DNA. (*b*) Domain motion of SHU in DNA binding. The fixed, moving and bending domains were identified by *DynDom* analysis. The α-helical body that is the fixed domain is represented in cyan and blue, and the β-ribbon arm that is the moving domain is shown in pink and red in apo SHU and in the SHU–DNA complex, respectively. The two regions of hinge-bending motion are shown in green. These results indicate the functional dynamics of SHU in DNA binding. The DNA binding also alters the distance between the DNA-binding β-ribbon arms. The distances between the tips of the DNA-binding β-ribbon arms are shown. The distance was measured between the C^{α} atoms of two Gln64 residues from each chain. (*c*) Side view and (*d*) top view of conformational changes of SHU upon DNA binding. Superposition of apo SHU and the SHU molecule of the SHU–DNA complex shows conformational changes in the β-ribbon arms of SHU, which move inwards upon DNA binding.

Table 4
Domain-motion parameters determined by *DynDom* for superposition of the different monomers of apo SHU and the SHU–DNA complex.

Apo–complex (chain)	*B*–*A*	*D*–*B*
Rotation angle (°)	37.1	36.5
Translation along axis (Å)	0.2	−0.5
% of closure motion	8.4	99.2
Bending region (residue Nos.)	53–55/74–76	54–55/74–76

r.m.s.d. value of 0.32 Å for the corresponding C^{α} atoms of residues 1–44 and 83–90. However, the other residues that show large deviations in the MD simulation undergo conformational changes upon DNA binding. The distances between the tips of the DNA-binding β-ribbon measured between the C^{α} atoms of the two Gln64 residues in a dimer changed from 39.6 Å in apo SHU to 47.9 Å in the SHU–DNA complex. The distances from chain *B* (apo) to chain *A* (complex) and from chain *D* (apo) to chain *B* (complex) are 10.9 and 14.7 Å, respectively (Fig. 5*b*).

The *DynDom* program (Hayward & Lee, 2002) was used to characterize the domain motion of SHU. The detailed degrees of bending and the hinge region between the apo and DNA-bound forms of SHU were compared. In the analysis, chains *B* and *D* of apo SHU and chains *A* and *B* of the SHU–DNA complex were used. The *DynDom* analysis recognized the α-helical body (blue in Fig. 5*b*) as the fixed domain and the β-ribbon arm (red in Fig. 5*b*) as the moving domain. The analysis also identified two regions of hinge-bending motion (green in Fig. 5*b*), namely Arg53–Arg55 and Ser74–Val76, which correspond to the residues identified in the r.m.s.f. analysis of the MD simulation. The salt bridge Lys75–Glu54, which connects two hinge regions, is disrupted by DNA binding, which suggests that Lys75 and Glu54 are pivotal residues in DNA bending and play essential roles in DNA binding. The rotation angle, translation, closure of moving domains with respect to the other domains and types of domains (fixed, moving and bending) are shown in Table 4.

3.3. DNA-binding properties of SHU revealed by EMSA and ITC

3.3.1. SHU binds to various DNAs. To assess the DNA-binding properties of SHU, several dsDNAs that were slightly modified from TR3 were designed as described in Supplementary Table S3. Although determining the dissociation constant was difficult owing to a lack of precision in the EMSA experiment, the binding-preference magnitude was determined based on the EMSA results. Firstly, SHU could bind several DNA substrates. Secondly, SHU preferentially binds to DNAs with distortion near the binding sites. The oligomer in which the unpaired T5 and T7 were removed (No. 5) showed decreased binding affinity compared with No. 7, which only has the unpaired T5 (Fig. 6). In a similar manner, SHU showed higher affinity for DNA No. 2, which has half unpaired T5 and T7, than for DNA No. 1, which is completely complementary (Fig. 6). Although the DNA kink is deliberately formed in this experiment, SHU preferentially recognizes the deformed DNA-like DNA kink which locally disrupts an otherwise linear helix. Additionally, this result demonstrates that the unpaired T5s contribute to the stabilization and acceleration of DNA binding between the nucleotides that form the kink. This DNA-recognition

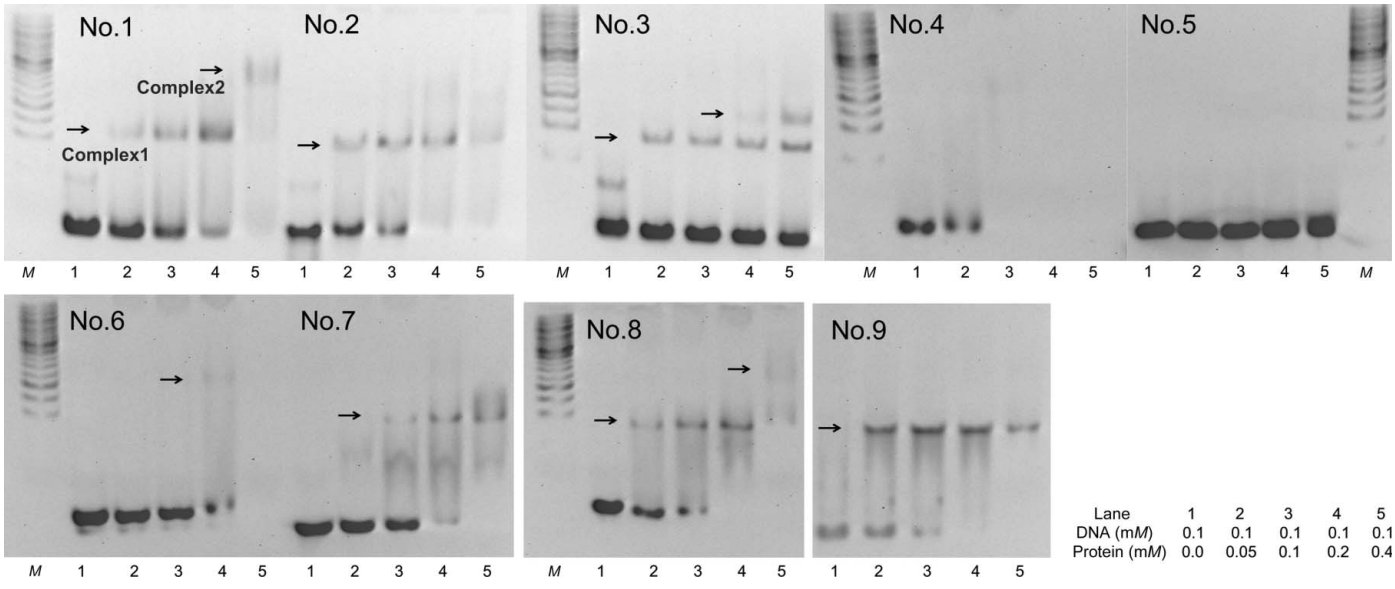

Figure 6
DNA-binding properties as determined from EMSA experiments. The binding of WT SHU to the various DNA duplexes is shown. The oligomers used in the assay are indicated at the top of each figure, and the sequences of the oligomers are listed in Supplementary Table S3. SHU protein at the concentrations indicated was mixed with DNA in a buffer containing 150 m*M* NaCl. Free and bound DNA were separated using 7%(*w*/*v*) nondenaturing polyacrylamide gels as described in §2. The details of the concentrations of protein and DNA in the lanes are indicated. The arrows indicate protein–DNA complexes at various ratios. As the concentration of SHU increases, additional recruitments of the SHU protein to pre-existing SHU–DNA complexes are observed. At the highest concentration of SHU (lane 5), the results were not clearly visible owing to smearing.

property supports the local shape-readout mechanism of SHU. Thirdly, to determine the preference for AT-rich regions, the central region (sequence 10–12) of TR3 was changed to ATT/TAA (No. 8) and to GCG/CGC (No. 9), respectively. A comparison of the binding affinity of SHU to DNAs Nos. 8 and 9 indicates that SHU binds to AT-rich and GC-rich regions with a similar affinity in the EMSA-scale experiment. Usually, AT-rich sequences of DNA are favoured by DNA-binding proteins because AT-rich DNA generally has more polar groups at the base edges (Jayaram *et al.*, 1989; Rohs *et al.*, 2010) and has a narrow minor-groove width (Rohs *et al.*, 2009) compared with GC-rich DNA, which increases the negative electrostatic potential of DNA through electrostatic focusing.

3.3.2. SHU binding-site size. Determining the size of the DNA-binding site is a prerequisite for understanding or predicting the mechanism of the function of DNA-binding proteins, which is essential for gene regulation. The DNA binding-site size can vary from six to 37 base pairs according to the length of the DNA and the experimental conditions (Bonnefoy & Rouvière-Yaniv, 1991; Wojtuszewski *et al.*, 2001; Swinger *et al.*, 2003).

To predict the size of the SHU binding site, EMSA experiments and studies of electrostatic properties were conducted (Huang, 2012; Ma *et al.*, 2011). For EMSA experiments, various lengths of oligomers [15-mer (No. 10), 21-mer (No. 1) and 35-mer (No. 11)] were used at different concentrations. Despite the 58% sequence identity, *T. maritima* HU and SHU showed different DNA-binding abilities. *T. maritima* HU with a ∼37 bp binding-site size did not form a complex with the 15-mer duplex (Grove & Lim, 2001), but complex formation was observed with the 15-mer duplex for SHU (Supplementary Fig. S5*a*).

Two complexes showing distinct mobilities are observed with the 15-mer and 21-mer duplexes (Supplementary Figs. S5*a* and S5*b*). Two distinct retardations are also observed with oligomer Nos. 1, 3 and 8 (Fig. 6). We surmise that SHU binds to DNA, resulting in the formation of complex 1. As protein concentrations increase, an increase in the fraction of complex 2 is observed. In binding to the 35-mer duplex, unstable complexes are observed rather than distinct complexes at higher concentrations of SHU. From the observation that SHU forms two complexes with 15 and 21 bp DNA, its binding-site size is estimated to be approximately 7–11 bp.

A predicted DNA-binding site was calculated using the *Patch Finder Plus* (*PFP*) web server (Shazman *et al.*, 2007) and is shown in Supplementary Fig. S7(*b*). The server predicted a large positive electrostatic patch on the protein surface, which generally corresponds to the residues involved in DNA binding.

From the combined results of the EMSA experiments, positively charged residue studies and *PFP* calculations, the DNA binding-site size of SHU is estimated to be 7–11 bp.

3.3.3. Binding affinities of WT SHU and SHU mutants for DNA. The interaction of SHU with TR3 was studied using ITC, and the results are shown in Fig. 2(*e*) and Supplementary S4(*c*). HU is known for nonspecific binding with relatively low affinity (K_d = ∼200–2500 n*M*) for undistorted dsDNA (Swinger *et al.*, 2003), but exhibits nonspecific binding with relatively high affinity (K_d = ∼2 n*M*) for distorted substrates (Kamashev & Rouviere-Yaniv, 2000). The DNA-binding reaction is exothermic and enthalpically driven, yielding a K_d of 370 ± 21 n*M*, and the binding stoichiometry (n) is approximately 1:1 for WT SHU, consistent with the crystal structure of the SHU–TR3 complex. The K_d shows relatively low affinity considering the distortion of TR3 and previous HU homologue studies. AHU demonstrates the highest affinity for dsDNAs that contain extended base pairs on both sides of TR3 (K_d of 13.0 ± 0.4 p*M*; Swinger & Rice, 2007). The affinity of AHU is 1000-fold higher than that of SHU, although the DNA sequences used in the experiments were different.

As mentioned in §3.1.3, five mutants, R55A, R58A, K59A, R61A and P63A, were constructed based on the protein–DNA interactions. Initially, EMSA experiments were conducted with TR3 (No. 6). However, we could not obtain a proper interpretation of these results (Supplementary Fig. S4*b*). Instead of EMSA experiments, we performed ITC experiments to compare the binding affinities of WT SHU and SHU mutants to TR3 (Supplementary Fig. S4*c* and Table 3). Additionally, EMSA experiments using DNA No. 2 were performed to measure the binding affinities of WT SHU and SHU mutants (shown in Supplementary Fig. S4*a*).

4. Discussion

4.1. β-Arm flexibility of SHU

HU, as one of the primary NAPs, could possess several roles that are related to DNA. Structural comparisons between each monomer from apo SHU and SHU–DNA have demonstrated the flexible nature of the SHU β-arms. The homologues also showed flexibility in their β-arms, revealing that this common feature is crucial in their role in DNA binding. These multiple conformations of HU according to β-arm orientation have also been revealed using NMR (Boelens *et al.*, 1996). We surmise that the flexible β-arms indicated by their multiple conformations enable SHU to serve as a 'biomolecular clamp' that recognizes the diverse configurations of DNA substrates and then negatively supercoils the DNA (Kannan *et al.*, 2014). Our MD simulations and *DynDom* analysis using apo SHU and SHU–DNA structures provided evidence for induced domain motion of SHU by DNA binding. Upon DNA binding, the hinge domain consisted of Arg53–Arg55 and Ser74–Val76 moved dynamically and resulted in a collapsed state of the β-arms. This motion was suggested to be a 'mechanical clamping' mechanism by Kannan *et al.* (2014).

To assess which residues contribute to the flexible nature of the β-arms, we mutated five residues in the β-arms and conducted ITC and EMSA experiments. The ITC and EMSA results corroborate one another, and the five mutants can be categorized into three groups. As the first group, R61A and P63A show the weakest binding to DNA, as indicated by the difficulty in determining the K_d value. The second group includes R55A and K59A, which exhibited increased K_d values and reduced binding affinities relative to WT SHU.

Despite its contribution in DNA binding, R58A demonstrated a small increase in K_d among the five mutants. Interestingly, we discussed Arg61 and Arg55 as the most energetically stable residues of the SHU–DNA complex as determined by free-energy analyses (§3.2.2), which suggests the essential role of these residues in DNA binding and recognition. In spite of its meaningful role in DNA binding from the ITC and EMSA results, Pro63 did not exhibit a significant free-energy change compared with those of Arg55 and Arg61. Although there is not much difference, Arg58 and Lys59 possess larger free-energy changes, possibly originating from the direct contact by hydrogen bonds to DNA bases. Thus, the arginine residues on the β-arms are essential for β-arm flexibility, which affects the DNA binding and hence the biological function.

4.2. SHU–DNA binding properties and the inferred biological function of SHU

Distinct substrate specificities according to species may be related to differing abilities to stabilize proline-mediated DNA kinks and salt bridges (Grove, 2011; Ma *et al.*, 2011; Mukherjee *et al.*, 2008). The proline-mediated DNA bend near T5 of the DNA is stabilized by the neighbouring Arg61 in SHU. This phenomenon is also observed in the AHU–DNA complex (Swinger *et al.*, 2003). The bent DNA with unpaired T5s that are 9 bp apart is preferred by SHU. The unpaired and flipped-out T7 near the kinks that makes the DNA require less energy for deformation also contributes to protein–DNA binding. The electrostatic surface view of SHU shows a positive stripe along the cradle-like area of the inner surface of the β-arms and the adjacent α-helical body (Supplementary Fig. S7*a*). Considering the size of this stripe, the DNA-binding site may be longer than 9 bp. Grove and coworkers revealed that the surface-exposed free Lys3, a highly conserved residue among HU homologues, is essential for determining the length of the binding DNA (Grove & Saavedra, 2002). In the case of *B. subtilis* phage SPO1 TF1 (PDB entry 1wtu) with ∼37 bp binding sites, the surface-exposed Lys3 has no close salt-bridge partner; thus, this Lys3 is predicted to interact with longer DNA (Kamau *et al.*, 2005). However, in the case of SHU the conserved Lys3 residue is positioned towards the inner side and forms a salt bridge to Asp26 which remained intact during the binding of SHU to dsDNA. The estimated DNA binding-site size of SHU from EMSA experiments is 7–11 bp, which is short compared with those of *E. coli* IHF (Meador *et al.*, 2008; Rice *et al.*, 1996) and *T. maritima* HU (Grove & Lim, 2001). Swinger and coworkers mentioned that the shortened DNA-binding site in the case of HU might be owing to crystal packing (Swinger *et al.*, 2003).

In our EMSA experiments, several lanes showed smearing or reduced DNA intensity, with various possible explanations. Firstly, the multiple nonspecific DNA binding of SHU may have various states of complexation at high concentrations of SHU, resulting in smearing. Secondly, the bimodal effects of HU might play a role depending on the protein concentration (Skoko *et al.*, 2004). At high SHU concentrations, compact SHU–DNA complex formation may inhibit access of the DNA dye, causing a gradual reduction in the DNA intensity, or the aggregates might fail to enter the gel. Thus, SHU at higher protein concentrations could exist as a very stable and compact aggregate that organizes and protects the genomic DNA, as demonstrated for other HU homologues (Mukherjee *et al.*, 2008; Ghosh & Grove, 2004). This phenomenon is biologically relevant to the persistence length of DNA (Nir *et al.*, 2011) and to supercoiling (Schnurr *et al.*, 2006). The possibility of a higher SHU population with DNA supports the previous findings of the relatively high concentration of HU in prokaryotic cells (30 000 dimers per cell; Rouvière-Yaniv & Kjeldgaard, 1979) and the gene-regulation function of HU (Prieto *et al.*, 2012).

In general, HU constrains the negative supercoiling of plasmid DNA (Broyles & Pettijohn, 1986; Grove, 2011), which is related to a change in linking number that depends on out-of-plane bending (writhe), underwinding of the helix at individual base-pair steps (twist), or both. Previously known structures of SHU homologue–DNA complexes show various characteristics in relation to negative supercoiling. AHU induces DNA underwinding and negative supercoiling. Hbb, a type II DNA-binding protein, also constrains negative supercoils, but exists in co-plane with DNA underwinding near the kinks (Mouw & Rice, 2007). IHF-bound DNA shows little net DNA unwinding and an inability to constrain negative DNA supercoiling. In SHU–DNA, out-of-plane bending with two kinks might constrain negative supercoiling. However, the DNA of the SHU–DNA complex exists nearly in co-plane, with a calculated dihedral angle of 8° compared with that of 40–73° for AHU–DNA complexes (Swinger *et al.*, 2003). At the kinks, dsDNA is overtwisted; however, this overtwisting is compensated by an undertwist angle near the kink site and the central 5 bps are overtwisted. The average twist angle was calculated to be 35° using the *w3DNA* web server (Zheng *et al.*, 2009) and is regarded as undertwisted compared with the twist angle of the canonical B-form DNA, which is approximately 37° (the Dickerson dodecamer is used as a representation of B-form DNA; Drew *et al.*, 1981). Therefore, SHU constrains negative supercoils but exists in near-co-plane with DNA underwinding near the kinks. This inferred role in constraining negative supercoiling suggests that SHU, as an NAP, affects the overall regulation of bacterial genomic expression.

4.3. The role of arginine residues in DNA binding

Rohs and coworkers suggest a new recognition mechanism that is explained by a narrow minor-groove width and by an enrichment in Arg in this region that compromises the base-readout and shape-readout mechanisms, which is also applicable to SHU. The Args in the β-arms of SHU, which are highly conserved in HU homologues, interact with the negatively charged region of DNA. Noticeably, Arg55 in the bending region of the β-arms is involved in binding in the central minor groove of DNA. Arg61 of the RNP motif penetrates the narrow minor groove near the kinks. Pro63 stacks in the kink and supports the DNA bending that would allow SHU to bind

DNA. The involvement of the Arg residues on the β-arms is universal in HU homologues. From EMSA and ITC experiments, we surmise that Arg55 and Arg61 are essential residues in DNA binding, although Arg55 and Arg61 are not completely conserved (Fig. 1*c*). Arg58 is conserved in all homologues and makes hydrogen bonds to DNA, but shows a relatively small affinity contribution to DNA binding.

The Arg residues are essential in recognizing the deformed B-DNA shape of TR3 in the minor groove. In the kink region, which is represented by a high roll angle and an overtwist, the Arg residues are directly involved in hydrogen-bonding and hydrophobic contacts. The Lys residues are also related to DNA interaction. In contrast to Arg, Lys forms water-mediated or direct hydrogen bonds to one nucleotide. Among the positively charged residues on the surface, an enrichment in Arg residues relative to Lys was observed in the SHU–TR3 interface. This prevalence is presumably owing to the higher energetic cost of removing a charged Lys from water compared with a charged Arg. Based on the SHU–DNA complex interface, the DNA-recognition mechanism of SHU presumably includes not only base readout but also shape readout, which is related to DNA shape and flexibility for DNA recognition.

Interestingly, all of the positive residues that form salt bridges in the complex structure are Lys rather than Arg residues. Holbrook and coworkers studied the IHF–DNA interaction using ITC and showed that the interaction is enthalpically driven (exothermic; Holbrook *et al.*, 2001). The authors proposed that DNA binding-coupled disruption of salt bridges is common in dsDNA or ssDNA wrapping/bending proteins such as IHF, HU, SSB, Lac repressor core tetramer and RNA polymerase (Holbrook *et al.*, 2001). Our data show that SHU undergoes salt-bridge disruption, which is energetically favoured when SHU binds to DNA. DNA-binding proteins utilize both salt-bridge disruption and salt-bridge formation coupled to nucleic acid binding at the interface. In the IHF–DNA complex, an Arg–Glu salt bridge forms at the DNA-binding interface. However, in the SHU–DNA complex no such salt bridges are present at the DNA-binding interface, presumably because all of the Arg residues are engaged in DNA binding.

4.4. Mechanism and implications for DNA recognition and binding of SHU

Two different plausible mechanisms of SHU–DNA complex formation can be considered. Either the DNA is partially pre-bent in the free state and then binds to free HU, or the DNA is bound to free HU and the DNA is then bent. The non-ideal structure of TR3 bound to SHU might be intrinsic to the DNA sequence or might be induced by the protein. Vivas and coworkers proposed that DNA molecules thermally fluctuate to adopt pre-bent conformations and are subsequently captured by multiple stabilizing protein–DNA interactions (Vivas *et al.*, 2012). Interestingly, previous MD simulation studies of CAP–DNA showed that the pre-bent DNA conformation partially exists in free DNA (Dixit *et al.*, 2005). MD simulations reveal that noncanonical DNA structures such as kinks and bubbles occur in mini-DNA circles (Lankaš *et al.*, 2006; Mitchell *et al.*, 2011). Previous studies and the results of this work suggest a possible mechanism of SHU–DNA complex formation (Supplementary Fig. S9). We surmise that SHU binds nonspecifically to the bent or kinked conformations of fluctuating DNA structures that are at least partially matched to the binding interface of the protein. In this step, the flexibility of the β-arms of SHU, which explains the large r.m.s.d.s between monomers, plays a crucial role in binding various DNAs. Then, to form the tightly bound complex, the SHU and DNA structures undergo mutually induced, energetically favoured conformational changes.

Although HU is known to have nonspecific DNA-binding characteristics, it has a binding preference for DNA. The mechanism for the recognition of DNA by HU is of interest because the protein–DNA recognition process is affected by multiple factors. Previously, the the DNA-recognition mechanism of HU was presumed to involve indirect readout, which relies on base pairs that are not directly contacted by the protein. Recently, the DNA-recognition mechanism has been considered to adopt base/shape readouts instead of direct/indirect readouts (Rohs *et al.*, 2010). The DNA recognition of SHU involves both shape and base readouts, and the specificity of binding is largely accomplished by DNA bending, kinking and intercalation, as described in previous sections. The residues on the β-arms recognize the bases of the minor groove of DNA through direct interactions such as hydrogen bonds or hydrophobic contacts.

This recognition mechanism is meaningful because the shape of the DNA, rather than the sequence of the DNA, plays a crucial role in SHU–DNA binding, and the specific DNA and protein properties are related to the recognition mechanism.

5. Conclusions

Studies of several other HU homologues have also revealed several biological functions of HU as a global gene regulator. HU binding to DNA facilitates higher order complex formation by allowing related factors to interact cooperatively with each other (Kar & Adhya, 2001; Chodavarapu *et al.*, 2008). For its biological function, it is essential for HU to recognize its target DNA with high affinity and specificity. Generally, a combined readout mechanism is involved in DNA recognition; however, the DNA-recognition mechanism of HU–DNA complex formation has been elusive. Therefore, elucidating the mechanism by which HU identifies and binds certain DNA is desirable. Our structural studies of apo SHU and the SHU–DNA complex suggest that the flexibility and the amino-acid residues of the β-arms are crucial for DNA recognition and binding, additionally representing not only basic biological features of HU, such as DNA bending and supercoiling, but also its dynamic features and DNA-binding mechanism. The results support a complex DNA-readout mechanism in which SHU forms hydrogen bonds in the minor groove (base

readout); however, this binding depends strongly on the DNA shape and flexibility (shape readout).

The development of antibiotics with novel modes of action is in high demand to combat multidrug-resistant bacteria. Because HU is a true gene regulator and is involved in various prokaryotic biological functions, such as transcription, DNA repair, virulence and the regulation of metabolism, blocking the activity of HU would damage bacterial survival. Furthermore, the DNA-replication machinery, which is conserved in bacteria, has recently been considered to be a potential drug target for the discovery of antibiotics with a novel mode of action (Robinson *et al.*, 2012). In this context, cross-talk between HU and other proteins, such as DnaA, OriC and topoisomerase I, is of interest. Because there is no antibacterial agent that targets the initiation process of DNA replication, developing inhibitors of the initiation of DNA replication could be a good strategy for seeking a new class of antibiotics. Recently, an inhibitor targeting the DNA binding of *M. tuberculosis* HU has been reported (Bhowmick *et al.*, 2014), which suggests the possibility of using SHU as a target for developing novel antibiotics. Our analysis of the apo SHU and SHU–DNA complex structures presents detailed characteristics of the DNA binding of SHU, providing valuable information for the development of novel antibiotics for MRSA and other bacteria that interfere with SHU dimerization or with SHU–DNA interactions.

6. Related literature

The following references are cited in the Supporting Information for this article: Burley & Petsko (1985) and Costantini *et al.* (2008).

The authors thank the beamline staff at Pohang Light Source (beamline 5C) in Korea and at SPring-8 (beamline 26B1) in Japan for assistance during X-ray experiments. This work was supported by PAL through the abroad beamtime program of the Synchrotron Radiation Facility Project under MEST, and the results were obtained using the RIKEN beamlines at Spring-8. This work was also supported by the National Research Foundation of Korea (NRF; grants 20070056817, 2012R1A2A1A01003569, NRF-2009-352-E00041 and 20110013663) funded by the Korean Government, Korea Healthcare Technology R&D Project, Ministry for Health, Welfare and Family Affairs, Republic of Korea (A092006) and the 2014 BK21 Project for Medicine, Dentistry and Pharmacy. The authors declare no conflict of interest in this work.

References

Adams, P. D. *et al.* (2010). *Acta Cryst.* D**66**, 213–221.
Avison, M. B., Bennett, P. M., Howe, R. A. & Walsh, T. R. (2002). *J. Antimicrob. Chemother.* **49**, 255–260.
Azam, T. A., Hiraga, S. & Ishihama, A. (2000). *Genes Cells*, **5**, 613–626.
Baker, T. A. & Kornberg, A. (1988). *Cell*, **55**, 113–123.
Berger, M., Farcas, A., Geertz, M., Zhelyazkova, P., Brix, K., Travers, A. & Muskhelishvili, G. (2010). *EMBO Rep.* **11**, 59–64.
Bewley, C. A., Gronenborn, A. M. & Clore, G. M. (1998). *Annu. Rev. Biophys. Biomol. Struct.* **27**, 105–131.
Bhowmick, T., Ghosh, S., Dixit, K., Ganesan, V., Ramagopal, U. A., Dey, D., Sarma, S. P., Ramakumar, S. & Nagaraja, V. (2014). *Nature Commun.* **5**, 4124.
Boelens, R., Vis, H., Vorgias, C. E., Wilson, K. S. & Kaptein, R. (1996). *Biopolymers*, **40**, 553–559.
Bonnefoy, E. & Rouvière-Yaniv, J. (1991). *EMBO J.* **10**, 687–696.
Bonnefoy, E., Takahashi, M. & Rouvière-Yaniv, J. (1994). *J. Mol. Biol.* **242**, 116–129.
Boubrik, F. & Rouviere-Yaniv, J. (1995). *Proc. Natl Acad. Sci. USA*, **92**, 3958–3962.
Broyles, S. S. & Pettijohn, D. E. (1986). *J. Mol. Biol.* **187**, 47–60.
Burley, S. K. & Petsko, G. A. (1985). *Science*, **229**, 23–28.
Case, D. A., Cheatham, T. E., Darden, T., Gohlke, H., Luo, R., Merz, K. M., Onufriev, A., Simmerling, C., Wang, B. & Woods, R. J. (2005). *J. Comput. Chem.* **26**, 1668–1688.
Castaing, B., Zelwer, C., Laval, J. & Boiteux, S. (1995). *J. Biol. Chem.* **270**, 10291–10296.
Chen, V. B., Arendall, W. B., Headd, J. J., Keedy, D. A., Immormino, R. M., Kapral, G. J., Murray, L. W., Richardson, J. S. & Richardson, D. C. (2010). *Acta Cryst.* D**66**, 12–21.
Chodavarapu, S., Felczak, M. M., Rouvière-Yaniv, J. & Kaguni, J. M. (2008). *Mol. Microbiol.* **67**, 781–792.
Christodoulou, E., Rypniewski, W. R. & Vorgias, C. R. (2003). *Extremophiles*, **7**, 111–122.
Christodoulou, E. & Vorgias, C. E. (1998). *Acta Cryst.* D**54**, 1043–1045.
Christodoulou, E. & Vorgias, C. E. (2002). *Extremophiles*, **6**, 21–31.
Costantini, S., Colonna, G. & Facchiano, A. M. (2008). *Bioinformation*, **3**, 137–138.
Dame, R. T. & Goosen, N. (2002). *FEBS Lett.* **529**, 151–156.
Dickerson, R. E. (1998). *Nucleic Acids Res.* **26**, 1906–1926.
Dillon, S. C. & Dorman, C. J. (2010). *Nature Rev. Microbiol.* **8**, 185–195.
Dixit, S. B., Andrews, D. Q. & Beveridge, D. L. (2005). *Biophys. J.* **88**, 3147–3157.
Dolinsky, T. J., Czodrowski, P., Li, H., Nielsen, J. E., Jensen, J. H., Klebe, G. & Baker, N. A. (2007). *Nucleic Acids Res.* **35**, W522–W525.
Drew, H. R., Wing, R. M., Takano, T., Broka, C., Tanaka, S., Itakura, K. & Dickerson, R. E. (1981). *Proc. Natl Acad. Sci. USA*, **78**, 2179–2183.
Drlica, K. (1992). *Mol. Microbiol.* **6**, 425–433.
Emsley, P. & Cowtan, K. (2004). *Acta Cryst.* D**60**, 2126–2132.
Engelhorn, M., Boccard, F., Murtin, C., Prentki, P. & Geiselmann, J. (1995). *Nucleic Acids Res.* **23**, 2959–2965.
Garvie, C. W. & Wolberger, C. (2001). *Mol. Cell*, **8**, 937–946.
Ghosh, S. & Grove, A. (2004). *J. Mol. Biol.* **337**, 561–571.
Gouet, P., Robert, X. & Courcelle, E. (2003). *Nucleic Acids Res.* **31**, 3320–3323.
Grimsley, G. R. & Pace, C. N. (2004). *Curr. Protoc. Protein Sci.*, Unit 3.1. doi:10.1002/0471140864.ps0301s33.
Grove, A. (2011). *Curr. Issues Mol. Biol.* **13**, 1–12.
Grove, A. & Lim, L. (2001). *J. Mol. Biol.* **311**, 491–502.
Grove, A. & Saavedra, T. C. (2002). *Biochemistry*, **41**, 7597–7603.
Guo, F. & Adhya, S. (2007). *Proc. Natl Acad. Sci. USA*, **104**, 4309–4314.
Hammond, J. B. & Kruger, N. J. (1988). *Methods Mol. Biol.* **3**, 25–32.
Hanaki, H., Kuwahara-Arai, K., Boyle-Vavra, S., Daum, R. S., Labischinski, H. & Hiramatsu, K. (1998). *J. Antimicrob. Chemother.* **42**, 199–209.
Hayward, S. & Lee, R. A. (2002). *J. Mol. Graph. Model.* **21**, 181–183.
Holbrook, J. A., Tsodikov, O. V., Saecker, R. M. & Record, M. T. Jr (2001). *J. Mol. Biol.* **310**, 379–401.
Howe, R. A., Bowker, K. E., Walsh, T. R., Feest, T. G. & MacGowan, A. P. (1998). *Lancet*, **351**, 602.

Huang, C.-Y. (2012). *Stoichiometry and Research – The Importance of Quantity in Biomedicine*, edited by D. A. Innocenti, p. 376. Rijeka: InTech.
Hwang, D. S. & Kornberg, A. (1992). *J. Biol. Chem.* **267**, 23083–23086.
Jayaram, B., Sharp, K. A. & Honig, B. (1989). *Biopolymers*, **28**, 975–993.
Jia, X., Grove, A., Ivancic, M., Hsu, V. L., Geiduscheck, E. P. & Kearns, D. R. (1996). *J. Mol. Biol.* **263**, 259–268.
Kamashev, D. & Rouviere-Yaniv, J. (2000). *EMBO J.* **19**, 6527–6535.
Kamau, E., Tsihlis, N. D., Simmons, L. A. & Grove, A. (2005). *Biochem. J.* **390**, 49–55.
Kannan, A., Camilloni, C., Sahakyan, A. B., Cavalli, A. & Vendruscolo, M. (2014). *J. Am. Chem. Soc.* **136**, 2204–2207.
Kar, S. & Adhya, S. (2001). *Genes Dev.* **15**, 2273–2281.
Lankaš, F., Lavery, R. & Maddocks, J. H. (2006). *Structure*, **14**, 1527–1534.
Lavery, R., Moakher, M., Maddocks, J. H., Petkeviciute, D. & Zakrzewska, K. (2009). *Nucleic Acids Res.* **37**, 5917–5929.
Li, J.-Y., Arnold-Schulz-Gahmen, B. & Kellenberger, E. (1999). *Microbiology*, **145**, 1–2.
Li, S. & Waters, R. (1998). *J. Bacteriol.* **180**, 3750–3756.
Lindorff-Larsen, K., Piana, S., Palmo, K., Maragakis, P., Klepeis, J. L., Dror, R. O. & Shaw, D. E. (2010). *Proteins*, **78**, 1950–1958.
Luscombe, N. M., Laskowski, R. A. & Thornton, J. M. (1997). *Nucleic Acids Res.* **25**, 4940–4945.
Ma, L., Sundlass, N. K., Raines, R. T. & Cui, Q. (2011). *Biochemistry*, **50**, 266–275.
Malik, M., Bensaid, A., Rouviere-Yaniv, J. & Drlica, K. (1996). *J. Mol. Biol.* **256**, 66–76.
Matthews, B. W. (1968). *J. Mol. Biol.* **33**, 491–497.
Meador, J. A., Zhao, M., Su, Y., Narayan, G., Geard, C. R. & Balajee, A. S. (2008). *Oncogene*, **27**, 5662–5671.
Miller, B. R., McGee, T. D., Swails, J. M., Homeyer, N., Gohlke, H. & Roitberg, A. E. (2012). *J. Chem. Theory Comput.* **8**, 3314–3321.
Mitchell, J. S., Laughton, C. A. & Harris, S. A. (2011). *Nucleic Acids Res.* **39**, 3928–3938.
Miyabe, I., Zhang, Q.-M., Kano, Y. & Yonei, S. (2000). *Int. J. Radiat. Biol.* **76**, 43–49.
Morales, P., Rouviere-Yaniv, J. & Dreyfus, M. (2002). *J. Bacteriol.* **184**, 1565–1570.
Morikawa, K., Ohniwa, R. L., Kim, J., Maruyama, A., Ohta, T. & Takeyasu, K. (2006). *Genes Cells*, **11**, 409–423.
Mouw, K. W. & Rice, P. A. (2007). *Mol. Microbiol.* **63**, 1319–1330.
Mukherjee, A., Sokunbi, A. O. & Grove, A. (2008). *Nucleic Acids Res.* **36**, 3956–3968.
Murshudov, G. N., Skubák, P., Lebedev, A. A., Pannu, N. S., Steiner, R. A., Nicholls, R. A., Winn, M. D., Long, F. & Vagin, A. A. (2011). *Acta Cryst.* D**67**, 355–367.
Nir, G., Lindner, M., Dietrich, H. R., Girshevitz, O., Vorgias, C. E. & Garini, Y. (2011). *Biophys. J.* **100**, 784–790.
Oberto, J., Nabti, S., Jooste, V., Mignot, H., Rouviere-Yaniv, J. & Imhof, A. (2009). *PLoS One*, **4**, e4367.
Otwinowski, Z. & Minor, W. (1997). *Methods Enzymol.* **276**, 307–326.
Otwinowski, Z., Schevitz, R. W., Zhang, R.-G., Lawson, C. L., Joachimiak, A., Marmorstein, R. Q., Luisi, B. F. & Sigler, P. B. (1988). *Nature (London)*, **335**, 321–329.
Pettersen, E. F., Goddard, T. D., Huang, C. C., Couch, G. S., Greenblatt, D. M., Meng, E. C. & Ferrin, T. E. (2004). *J. Comput. Chem.* **25**, 1605–1612.
Pontiggia, A., Negri, A., Beltrame, M. & Bianchi, M. E. (1993). *Mol. Microbiol.* **7**, 343–350.
Preobrajenskaya, O., Boullard, A., Boubrik, F., Schnarr, M. & Rouvière-Yaniv, J. (1994). *Mol. Microbiol.* **13**, 459–467.
Prieto, A. I., Kahramanoglou, C., Ali, R. M., Fraser, G. M., Seshasayee, A. S. & Luscombe, N. M. (2012). *Nucleic Acids Res.* **40**, 3524–3537.
Rice, P. A., Yang, S., Mizuuchi, K. & Nash, H. A. (1996). *Cell*, **87**, 1295–1306.
Robinow, C. & Kellenberger, E. (1994). *Microbiol. Rev.* **58**, 211–232.
Robinson, A., Causer, R. J. & Dixon, E. (2012). *Curr. Drug Targets*, **13**, 352–372.
Rohs, R., Jin, X., West, S. M., Joshi, R., Honig, B. & Mann, R. S. (2010). *Annu. Rev. Biochem.* **79**, 233–269.
Rohs, R., West, S. M., Sosinsky, A., Liu, P., Mann, R. S. & Honig, B. (2009). *Nature (London)*, **461**, 1248–1253.
Roth, A., Urmoneit, B. & Messer, W. (1994). *Biochimie*, **76**, 917–923.
Rouvière-Yaniv, J. & Gros, F. (1975). *Proc. Natl Acad. Sci. USA*, **72**, 3428–3432.
Rouvière-Yaniv, J. & Kjeldgaard, N. O. (1979). *FEBS Lett.* **106**, 297–300.
Schnurr, B., Vorgias, C. & Stavans, J. (2006). *Biophys. Rev. Lett.* **1**, 29–44.
Scopes, R. K. (1974). *Anal. Biochem.* **59**, 277–282.
Semsey, S., Virnik, K. & Adhya, S. (2006). *J. Mol. Biol.* **358**, 355–363.
Serban, D., Benevides, J. M. & Thomas, G. J. Jr (2003). *Biochemistry*, **42**, 7390–7399.
Shazman, S., Celniker, G., Haber, O., Glaser, F. & Mandel-Gutfreund, Y. (2007). *Nucleic Acids Res.* **35**, W526–W530.
Skarstad, K., Baker, T. A. & Kornberg, A. (1990). *EMBO J.* **9**, 2341–2348.
Skoko, D., Wong, B., Johnson, R. C. & Marko, J. F. (2004). *Biochemistry*, **43**, 13867–13874.
Sugino, A., Peebles, C. L., Kreuzer, K. N. & Cozzarelli, N. R. (1977). *Proc. Natl Acad. Sci. USA*, **74**, 4767–4771.
Swinger, K. K., Lemberg, K. M., Zhang, Y. & Rice, P. A. (2003). *EMBO J.* **22**, 3749–3760.
Swinger, K. K. & Rice, P. A. (2007). *J. Mol. Biol.* **365**, 1005–1016.
Tanaka, I., Appelt, K., Dijk, J., White, S. W. & Wilson, K. S. (1984). *Nature (London)*, **310**, 376–381.
Travers, A. A. (1989). *Annu. Rev. Biochem.* **58**, 427–452.
Ussery, D., Schou Larsen, T., Wilkes, K. T., Friis, C., Worning, P., Krogh, A. & Brunak, S. (2001). *Biochimie*, **83**, 201–212.
Van Der Spoel, D., Lindahl, E., Hess, B., Groenhof, G., Mark, A. E. & Berendsen, H. J. (2005). *J. Comput. Chem.* **26**, 1701–1718.
Vis, H., Mariani, M., Vorgias, C. E., Wilson, K. S., Kaptein, R. & Boelens, R. (1995). *J. Mol. Biol.* **254**, 692–703.
Viswamitra, M. A., Kennard, O., Jones, P. G., Sheldrick, G. M., Salisbury, S., Falvello, L. & Shakked, Z. (1978). *Nature (London)*, **273**, 687–688.
Vivas, P., Velmurugu, Y., Kuznetsov, S. V., Rice, P. A. & Ansari, A. (2012). *J. Mol. Biol.* **418**, 300–315.
Wang, G., Lo, L. F. & Maier, R. J. (2012). *DNA Repair (Amst.)*, **11**, 733–740.
White, S. W., Appelt, K., Wilson, K. S. & Tanaka, I. (1989). *Proteins*, **5**, 281–288.
White, S. W., Wilson, K. S., Appelt, K. & Tanaka, I. (1999). *Acta Cryst.* D**55**, 801–809.
Winn, M. D. *et al.* (2011). *Acta Cryst.* D**67**, 235–242.
Wojtuszewski, K., Hawkins, M. E., Cole, J. L. & Mukerji, I. (2001). *Biochemistry*, **40**, 2588–2598.
Zheng, G., Lu, X.-J. & Olson, W. K. (2009). *Nucleic Acids Res.* **37**, W240–W246.